ELSEVIER

Journal of Structural Geology 27 (2005) 1069–1094

JOURNAL OF STRUCTURAL GEOLOGY

www.elsevier.com/locate/jsg

Growth of syndepositional faults in carbonate strata: Upper Permian Capitan platform, New Mexico, USA

Eduard Koša[a,*], David W. Hunt[a,b]

[a]*Department of Earth Sciences, University of Manchester, Oxford Road, Manchester, UK*
[b]*Norsk Hydro, Oil and Energy Research Centre, Bergen, P.O. Box 7190-N5020 Bergen, Norway*

Received 3 March 2004; received in revised form 10 February 2005; accepted 21 February 2005
Available online 17 June 2005

Abstract

The Upper Permian Capitan platform, New Mexico, is cut by syndepositional faults and fractures. These are parallel to platform margin and cluster within strata that steepen and thicken abruptly into the basin. Faults are steep, dip-slip, have measurable displacements of up to 24 m, are typically associated with growth strata, and mostly tip-out blindly within the platform. Basinward-throwing faults are typically reverse, and are steeper than shelfward-throwing faults, which have normal geometry. The sense of displacement across some initially basinward-throwing faults changed as they developed. These patterns indicate that faults were rotated as they grew. Synkinematic rotation of faults is interpreted to have occurred due to syndepositional, compaction-driven, down-to-basin tilting of the Capitan platform. Faults grew through interaction with inherited fractures and by segment linkage. Vertically separated fault segments had a tendency to grow downward to link with underlying segments, thus promoting accumulation of displacement across faults without vertical propagation of fault tips. Four fault types are distinguished on the basis of structures associated with their upper terminations: (I) faults breaking free surface, (II) faults tipping out within non-folded growth strata, (III) faults tipping out below growth monoclines, and (IV) buried faults with no expression on free surface. Fault tips evolved from one type into another in response to variations in the rates of fault growth and deposition. Fault-tip structures also vary laterally over distance of 750–1400 m, inferably as a result of variable distances from fault centres.

Keywords: Syndepositional fault; Fault segment; Fracture; Growth fold; Differential subsidence; Deposition

1. Introduction

In the last two decades, significant advances have been made in understanding how extensional faults grow and link together from initially isolated segments. To date, most of these studies have focused on tectonic faults in siliciclastic rocks (e.g. Peacock and Sanderson, 1991; Walsh and Watterson, 1992; Anders and Schlische, 1994; Childs et al., 1996; Peacock and Sanderson, 1996; Ferrill et al., 1999; Walsh et al., 1999). Various studies have shown that faults in lithified rocks may differ in terms of scale and faulting mechanisms from faults developed within non-lithified sediments (Jackson and McKenzie, 1983; Muraoka and Kamata, 1983; Wibberley et al., 1999; Hunt et al., 2002). Syndepositional faults develop in interaction with sedimentation, and are commonly associated with growth strata (Leeder and Gawthorpe, 1987; Gawthorpe et al., 1994, 1997; Doglioni et al., 1998; Rosales et al., 1994; Schlische and Anders, 1996; Rosales, 1999; Gawthorpe and Leeder, 2000; Vergés et al., 2002). The thickness, sedimentary facies and geometry of growth strata may provide important information on the rates, timing and processes of syndepositional faulting (Burchette, 1988; Chronis et al., 1991; Cross et al., 1998; Wilson, 1999; Graziano, 2000; Kkjennerud et al., 2001). In contrast, no comparable constraints are available for studies of faults that are not associated with growth strata (Bertram and Milton, 1989; Doglioni et al., 1998; Bosence et al., 1998).

The Upper Permian Capitan platform in the Guadalupe Mountains, New Mexico, USA, is cut by closely spaced syndepositional faults and fractures (Figs. 1 and 2; Hunt et al., 2002; Koša et al., 2003). Most of these syndepositional faults tip out blindly within the platform, are associated with

* Corresponding author. Current address: Shell UK Ltd, 1 Altens Farm Rd, Nigg, Aberdeen AB12 3FY, UK.
E-mail address: eduard.kosa@shell.com (E. Koša).

0191-8141/$ - see front matter © 2005 Elsevier Ltd. All rights reserved.
doi:10.1016/j.jsg.2005.02.007

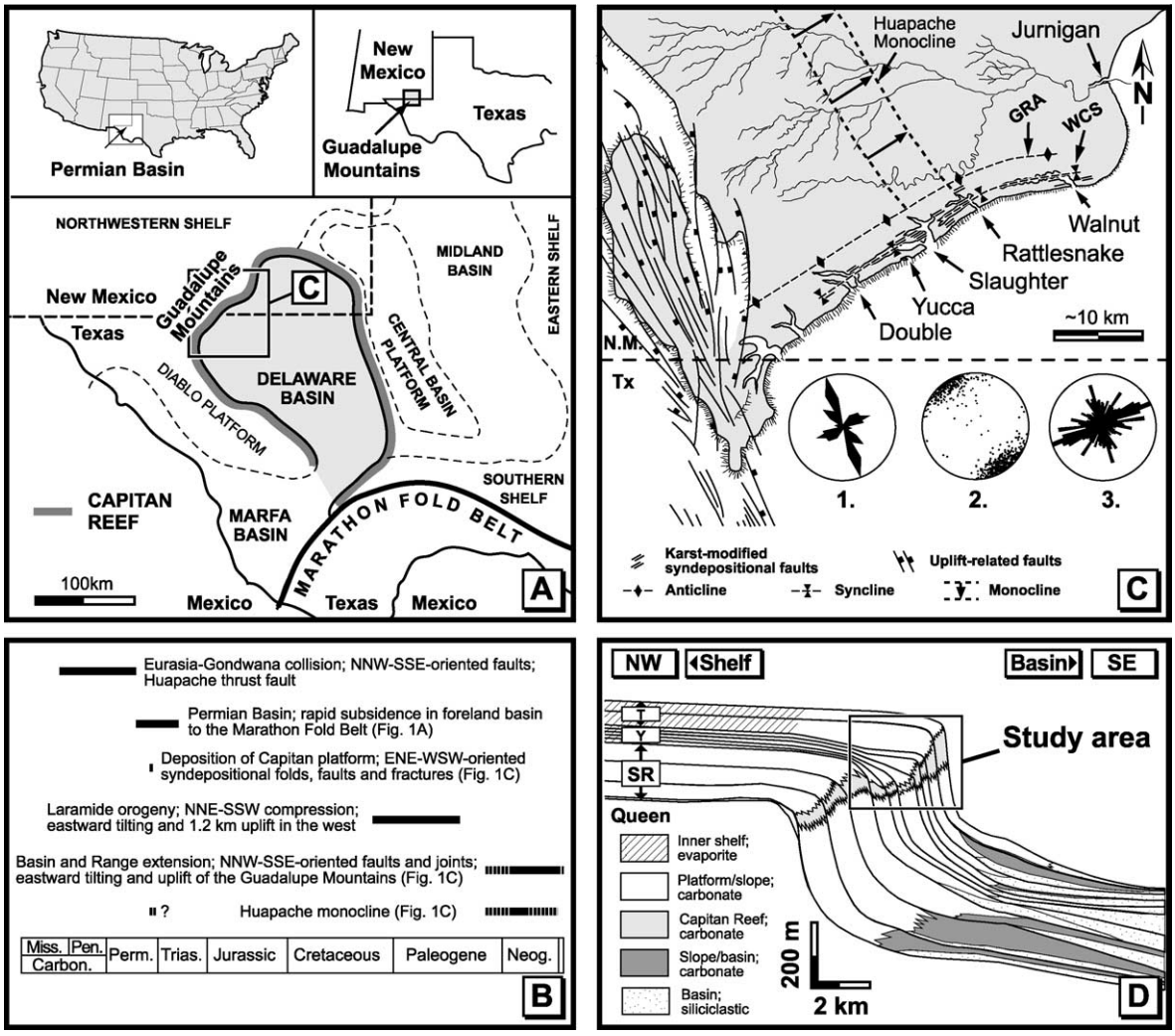

Fig. 1. Location and geology of the study area. (A) Regional setting. (B) Timing and nature of main structural events impacting on the Upper Permian Capitan platform (modified after Hill, 2000). (C) The Guadalupe Mountains, Texas and New Mexico. The range is uplifted along NNW–SSE-trending faults. The SE escarpment represents the exhumed platform margin. Syndepositional faults and folds parallel the platform margin. Stereonets show orientation of uplift-related faults and fractures (1), syndepositional faults and fractures (2) (Fig. 2), and trends of fault- and fracture-controlled passages of Lechuguilla Cave (3). GRA, Guadalupe Ridge anticline; WCS, Walnut Canyon syncline; (D) Stratigraphic cross-section through the Capitan platform. Composite depositional sequences: SR, Seven Rivers; Y, Yates; T, Tansill (after Kerans et al., 1992).

growth strata, and have displacement of less than 24 m. Owing to the relatively small displacement, fine-scale features of juvenile-stage fault evolution are preserved. The faults thus show geometries and patterns that are likely to have characterised early stages of growth of the more commonly studied, larger-scale faults. In particular, features related to fault growth by interaction with inherited fractures, and by linkage of isolated fault segments, are revealed in great detail. Growth strata and sediments filling fault and fracture voids can be used to establish the timing of faulting and fracturing with a high degree of confidence. In addition, exposures of same faults and fractures that can be studied on opposite sides of a 750–1400-m-wide canyon cutting the platform perpendicularly to depositional strike also permit to observe lateral structural variations (Fig. 2).

This paper builds out from our earlier studies of the Capitan platform that focused on the influence of syndepositional faulting on platform deposition and stratigraphy (Hunt et al., 2002) and on structure-controlled palaeokarst (Koša et al., 2003). This paper focuses exclusively on structural aspects of syndepositional faults and fractures in the Capitan platform. Structural characteristics of faults and fractures are described, and are interpreted in terms of their spatial and temporal heterogeneity. Faults are shown to have grown in interaction with inherited passive fractures and through segment linkage. Evolution of growth folds above fault tips is also discussed. Interaction between rates of differential subsidence and platform aggradation are shown to have controlled the temporal evolution of fault-tip structures. Implications of the study for structural evolution of the Capitan platform are discussed. Finally, the results of

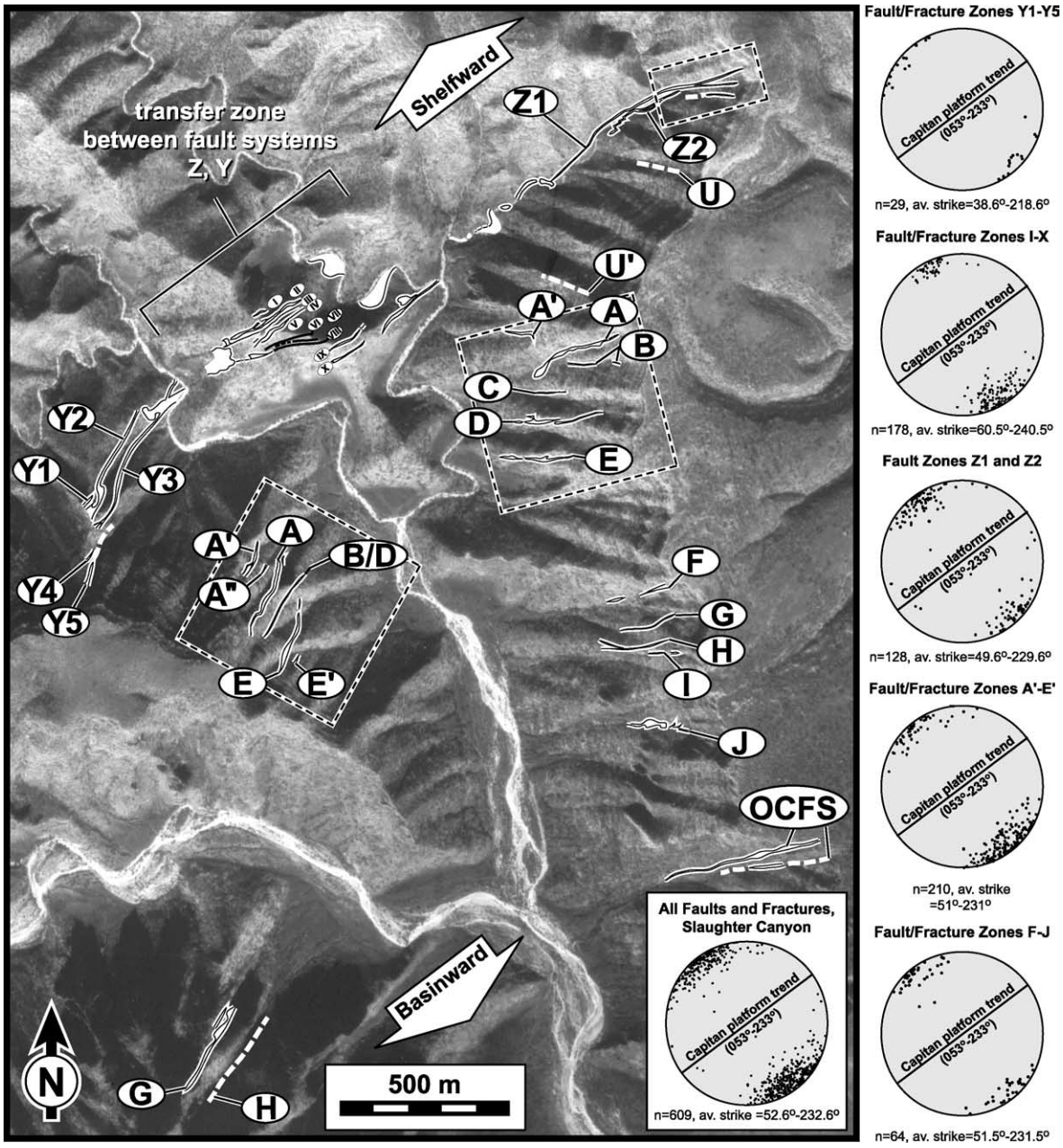

Fig. 2. Aerial photograph of Slaughter Canyon showing the 22 fault zones and 13 major fractures studied (white). Faults and fractures trend parallel to Capitan platform margin (Fig. 1B). Dotted squares indicate areas and structures discussed in detail.

this study are compared with some other studies of syndepositional faults.

2. Geologic setting

2.1. Structural evolution

The Permian Basin in western Texas and southeastern New Mexico has evolved as a foreland basin to the Marathon Fold Belt, which was formed during the continental collision between Laurasia and Gondwana in the late Mississippian–early Permian (Fig. 1A; Hill, 1996, 2000). Three major stages of tectonic deformation are recognised in the basin (Fig. 1B). (i) Early in its evolution, NNW–SSE-trending faults divided the incipient Permian Basin into three parts: Midland Basin, Central Basin Platform and Delaware Basin (Fig. 1A). (ii) The Late Cretaceous through Eocene Laramide orogeny caused compressional deformation in parts of the basin, and resulted in uplift of ca. 1.2 km of its western side (Erdlac, 1993; Hill, 1996). (iii) The final stage of deformation involved km-scale movements along NNW–SSE-oriented faults related to the Basin and Range uplift and extension in

the Oligocene–Pliocene (Hayes, 1964; Garber et al., 1989; Hill, 1996, 2000).

The Guadalupe Mountains represent the easternmost range of the Basin and Range Province (Fig. 1C). Strata in the range dip slightly (1–2°) to the east. The Upper Permian Capitan platform, which rims the Delaware Basin (Fig. 1A), is superbly exposed along the SE escarpment of the range (Fig. 1C and D). Although devoid of significant structural complexity, the platform records several episodes and regimes of deformation. Firstly, the outer part of the platform was subject to syndepositional down-to-basin tilting associated with folding, faulting and fracturing. This tilting is considered to have been driven by differential compaction of underlying fine-grained siliciclastic basinal sediments (Fig. 1D; Saller, 1996; Longley, 1999; Hunt et al., 2002). Syndepositional folds, faults and fractures parallel the platform margin, extend for at least 33 km along-strike between Double and Walnut canyons, and are known to exist within the outermost 5–6 km of the platform (Fig. 1C; Koša et al., 2003). Exposures of some of these syndepositional folds, faults and fractures in Slaughter Canyon of the Guadalupe Mountains are examined by this study (Figs. 1C and 2).

Post-depositional deformation of the Capitan platform is minor, and includes small-scale faults, fractures and flexures perpendicular to the platform margin. In the westernmost part of the Guadalupe Mountains, these normal faults and joints are related to uplift of the range in Oligocene–Pliocene (Fig. 1C). In the study area in North Slaughter Canyon, centimetre-scale normal faults and joints perpendicular to the platform margin are most likely to be related to the NNW–SSE-trending, ENE-dipping Huapache monocline (Fig. 1C). The monocline has approximately 150 m of relief between Slaughter and Rattlesnake canyons, and is interpreted to have formed through drape–folding of strata over the basement-seated Huapache thrust-fault of primarily Pennsylvanian–Wolfcampian age (Hayes, 1964; Jagnow and Jagnow, 1992; Hill, 1996).

2.2. Capitan platform architecture and deposition

The Capitan platform is a reef-rimmed, mixed evaporite–carbonate–siliciclastic shelf with progradational/aggradational geometry (Fig. 1D). Cyclic sedimentation on the platform was controlled by high-frequency sea-level oscillations (Meissner, 1972; Mazzullo et al., 1985; Fischer and Sarnthein, 1988; Sarg, 1988; Borer and Harris, 1989; Kerans et al., 1992; Saller et al., 1999). At least three orders of depositional cyclicity are readily recognised, and are identified in terms of sequence stratigraphy (Fig. 3). A depositional sequence is defined as a sedimentary unit deposited during a single cycle of a relative sea-level movement of a certain order, and is bound by sequence boundaries representing the lowest stands of the relative sea level during that cycle. The Seven Rivers, Yates and Tansill stratigraphic units represent the highest, 3rd-order, depositional sequences. These consist of 4th-order, high-frequency sequences (HFS), including the Seven Rivers 1–4, Yates 1–4 and Tansill 1–2 HFSs (Osleger, 1998; Tinker, 1998; Kerans and Tinker, 1999; Hunt et al., 2002). In the study area, individual HFSs are ca. 30–80 m thick, and are composed of metre-scale, 5th- and lower-order cycles. Highstand carbonate lithologies dominate the cycles, and are commonly punctuated by minor lowstand siliciclastics deposited upon subaerially exposed sequence boundaries (e.g. Osleger, 1998; Tinker, 1998; Hunt et al., 2002).

Estimates for the duration of individual 4th-order HFSs range between 250 and 400 ka (Borer and Harris, 1989, 1991, 1995; Osleger, 1998; Tinker, 1998). Duration of the 5th-order cycles is estimated to have ranged between 20 and 100 ka (Borer and Harris, 1989, 1991, 1995; Ye and Kerans, 1996; Osleger, 1998; Tinker, 1998; Hunt et al., 2002). The rate of platform aggradation in Slaughter Canyon is estimated to have ranged from 0.053 to 0.336 m/ka during deposition of the Yates composite sequence (Hunt et al., 2002).

3. Methods

In the field syndepositional folds, faults and related fracture systems have been systematically mapped onto 1:8000 aerial photographs, 1:50 scale photomosaics and 1:10 Polaroid photographs. Structural dip and dip-direction data have been collected from fault and fracture planes, as well as from walls of palaeocaverns developed along them. The stratigraphic framework of the faulted platform has been constrained by walking out and mapping the main stratal surfaces and facies tracts onto 1:50 scale photomosaics. As this was done, bedding and geopetal data were also collected from the platform strata. The resulting integrated structural and stratigraphic framework is constrained by 13, 1:25 scale logged stratigraphic sections.

Methodologies and parameters used to quantify fault growth are illustrated in Fig. 4. Stratigraphic sections measured on either side of faults have been used to correlate stratigraphic surfaces, and to quantify differential subsidence across faults (Fig. 1A and B). Thickness and facies variations of strata across faults have been used to identify growth strata: depositional units where thickness and facies are uniform across faults are considered non-growth, while those showing thickness and (in some instances) facies variations across faults are taken to represent growth strata. Most of the studied faults are associated with growth folds. Horizon separations measured directly on faults cutting through growth folds are lower than the total across-fault differential subsidence (Fig. 4A). Therefore, differential subsidence measured away from the growth folds, rather than displacement measured directly on fault traces, is used here to quantify fault movement. This method also permits quantification of differential subsidence across growth monoclines that have not been penetrated by a fault. Differential subsidence/distance plots were constructed

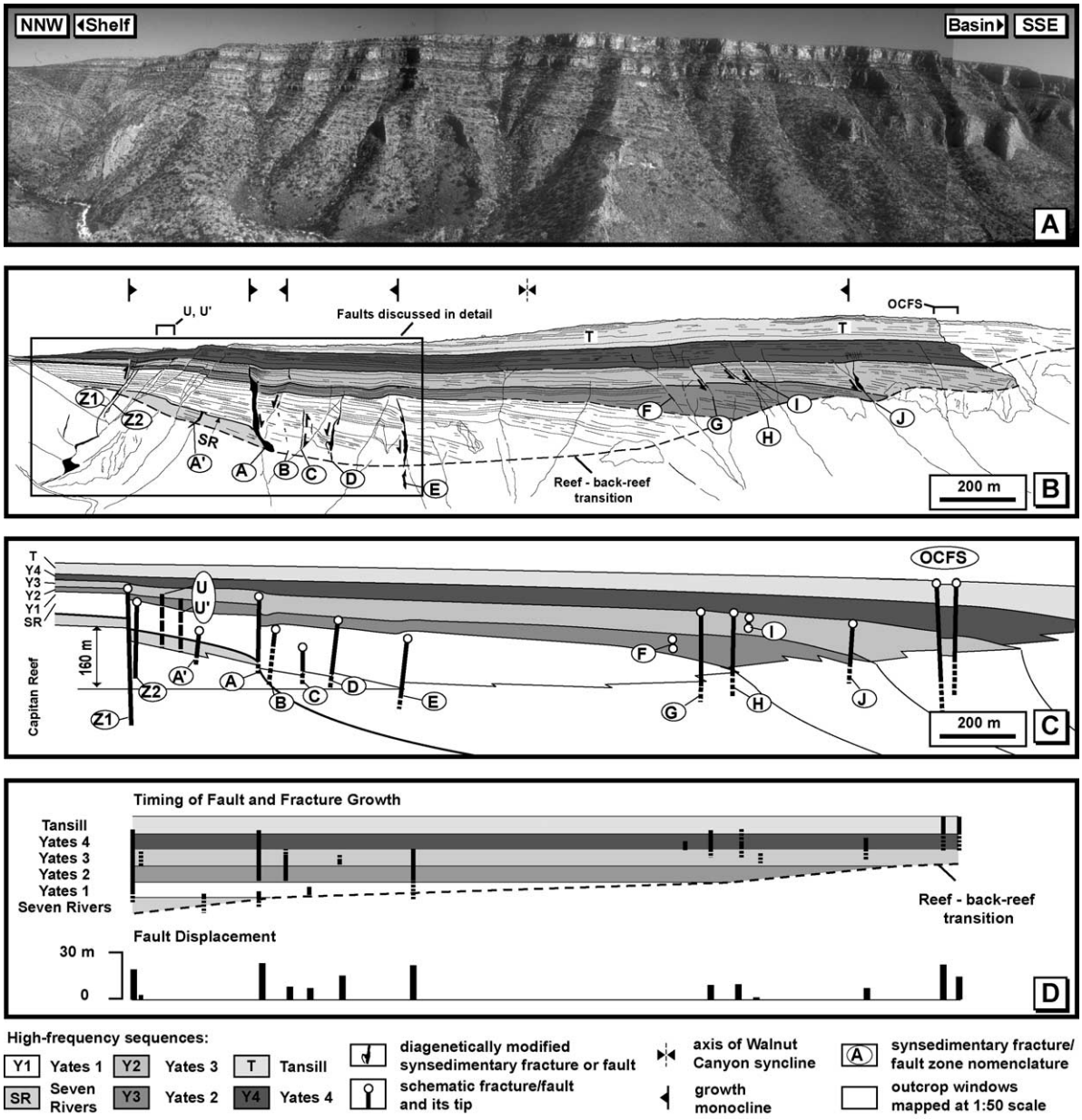

Fig. 3. Photograph (A), line drawing (B), and a schematic reconstruction (C) of a 2.6 km dip section through the Capitan platform on the eastern side of Slaughter Canyon. The timing of fault growth and throw are summarised in (D). Note the basinward dip and divergence of shelf strata towards the basin, and the apparent down stepping of the reef to back-reef transition by ca. 160 m between faults Z1 and A. These patterns are interpreted to have formed by compaction-driven syndepositional down-to-basin tilting of the outer platform strata. Faults and fractures are clustered in areas characterised by abrupt steepening of strata.

using measured-section data, whereby differential subsidence data were plotted against distances measured from upper fault tips to surfaces within hanging walls (Fig. 4B).

Hunt et al. (2002) calculated displacement rates and fault-tip-propagation rates to quantify *growth over time* of five faults in the Capitan platform. A different methodology has been applied in this study. *Growth differential subsidence (GDS)*, rather than fault propagation, is used here to quantify *fault movement related to deposition* (Fig. 4C). This methodology has been chosen as field observations revealed that faults could accumulate displacement, and influence surface topography, without vertical propagation of their upper tips. Examples of such faults are shown in Fig. 4D and E, and are illustrated in detail later in the paper. *Growth differential subsidence (GDS)* is measured as the vertical distance, in metres, between the base of growth strata in the hanging wall and the fault tip. *Platform aggradation (A)* is the vertical thickness, in metres, of a stratigraphic unit. *Growth-differential-subsidence/platform-aggradation ratio (GDS/A)* is a measure of fault movement related to contemporaneous deposition, whereby *GDS/A* equals the vertical distance between the base of growth strata in hanging wall and fault tip, divided by the hanging wall thickness of growth strata deposited during

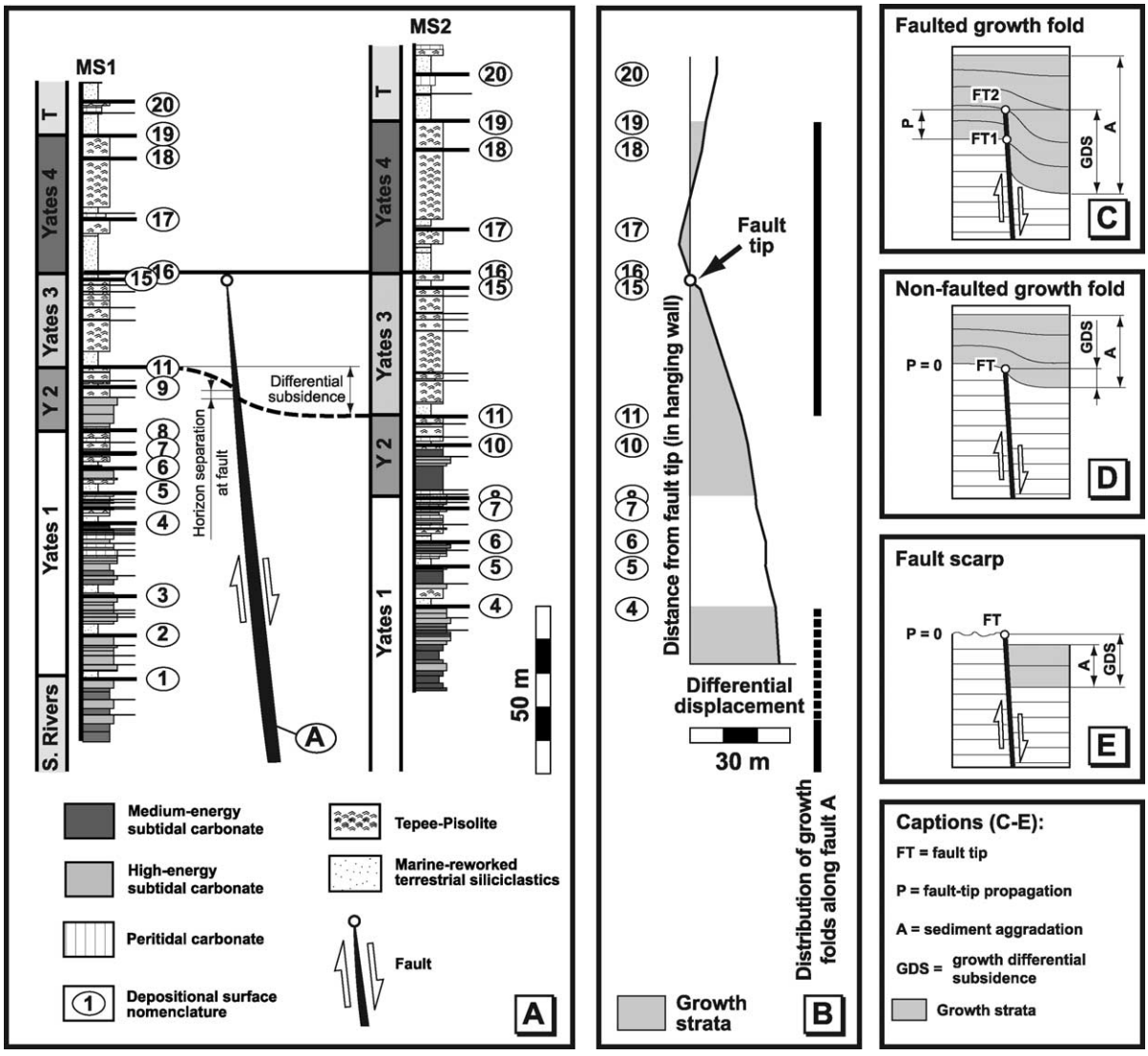

Fig. 4. Examples of data and methods used to constrain the timing and rates of fault evolution. (A) Measured section data constrain the timing of fault A, east side, North Slaughter Canyon. (B) Differential subsidence/distance curve constructed for fault A on the basis of measured section data. Distribution of growth strata and fault-related growth folds is indicated. (C)–(E) Methodology used to constrain growth differential subsidence/platform aggradation ratios illustrated on schematic examples of three different fault configurations.

the examined *GDS* event. The *GDS/A* ratio thus represents a dimensionless number, and is independent of estimates of the time-duration of fault movement and deposition.

Note that for the sake of simplicity *GDS/A* ratios have been calculated using thicknesses and distances measured on outcrop. These data do not take into consideration the effects of compaction.

4. General characteristics of syndepositional faults and fractures

4.1. Structure

Syndepositional faults and fault-related fracture systems in the Capitan platform have a very consistent orientation, and trend parallel to depositional strike of the Capitan platform (052.6–232.6°; $n = 609$; Figs. 1C and 2). In map-view, fault zones are laterally segmented across a range of scales. In cross-section, two types of syndepositional structures are readily recognised: (i) passive dilatational fissures with no discernible displacement, and (ii) faults. *Passive fissures* are up to 40 m deep, commonly widen upward, and tip out abruptly below sequence boundaries. Strata above such upward-opening fissures are typically deformed into narrow growth synclines, and are commonly brecciated, or even partly collapsed, into the fissures. *Faults* have vertical extent of at least 270 m and displacements of up to 24 m as measured in back-reef strata (average 10 m; Fig. 3). The maximum displacements cannot however, be established with certainty due to the lack of stratigraphic markers within the massive Capitan reef that forms the

lower part of the outcrop (Fig. 3). In dip sections, faults commonly consist of en-échelon segments, many of which are linked across prominent fault bends. Restraining bends are most common. Slickensides and offset reveal that all syndepositional faults are dip slip (Hunt et al., 2002). Evidence for reworking of fault fabrics and deposits within fault and fracture zones is ubiquitous, and indicates repeated fracturing and fault reactivation (Koša et al., 2003).

4.2. Distribution

Syndepositional faults and fractures are not distributed randomly within the platform (Fig. 3). Instead, they tend to be clustered within strata that steepen and thicken abruptly basinward. Strata within the Yates 1 HFS thicken by 90% between faults Z1 and E. This thickening is associated with dips of up to 16° of the Yates 1 strata, and also with deflection of the reef/back-reef transition downward by approximately 160 m. Similarly, fracture F and faults G–I are developed where back-reef strata of the Yates 2 HFS become steeper and thicken abruptly basinward. And in a similar way, fault J is located where the Yates 3 HFS strata thicken abruptly and steepen by up to 8° (Fig. 3). Faults and fractures appear to become progressively younger, shorter-lived, and to reach higher stratigraphic levels, basinward (Fig. 3D).

4.3. Karst-modification

Syndepositional faults and fractures in the Capitan platform localised early karst, resulting in the development of penetrative karst systems along them (Hunt et al., 2002; Koša et al., 2003). Most palaeocaverns are steep, have a sheet-shaped external form, and are generally less than 10 m wide (e.g. Fig. 5). Irregular-shaped palaeocaverns also exist, and may be up to 90 m wide, but are relatively rare (e.g. palaeocaverns within transfer zone between fault systems Z1–Z2 and Y1–Y5; Fig. 2). Although modification by dissolution is important, it has been normally localised within faults and fractures, so that most of their original segmentation and structural heterogeneity is maintained (e.g. Fig. 5). However, because of the dissolution, little primary fault and fracture rock remains within the fault and fracture zones. Instead, rocks within the fault- and fracture-related palaeocaverns are predominantly of sedimentary origin (Hunt et al., 2002; Koša et al., 2003).

4.4. Evidence for syndepositional origin

Various lines of evidence demonstrate the syndepositional nature of the studied faults, fractures and related folds. The main *structural* and *sedimentologic* evidence may be illustrated on the example of faults A and B in Fig. 5: (i) faults tip-out below growth folds, (ii) conjugate faults bound growth troughs and synclines, (iii) up to 55% thickness changes of individual HFSs are observed across faults, and are associated with facies changes, (v) erosional truncation and by-pass surfaces occur on footwall crests of faults that have breached the top of the platform, (vi) soft-sediment deformation features are found within growth folds and in strata overlying passive fissures.

The structural and sedimentologic evidence for syndepositional origin of faults and fractures is supplemented by *diagenetic* and *palaeontologic* criteria. Faults and fractures served as conduits for dolomitising fluids formed by evaporation in the inner-platform lagoon (Melim and Scholle, 2002; Hunt et al., 2002; Koša et al., 2003). Penetrative karst systems developed along faults and fractures, and are filled by early marine cements and platform-derived sediments. The sediments are mostly matrix- to clast-supported breccias, and commonly contain carbonate particles such as coated grains, peloids and bioclasts of Capitan-age organisms. Our previous work (Hunt et al., 2002; Koša et al., 2003) demonstrated that sediments were introduced into the faults, fractures and palaeocaverns from above, therefore the fills can be tied to deposition on platform top.

5. Syndepositional faults and fractures, North Slaughter Canyon

In this study, attention is focused on faults and fractures Z1–E exposed in North Slaughter Canyon (Fig. 2). Faults Z1 and Z2 are exposed within a 150 m high face of a NE branch of North Slaughter Canyon, and can be traced along-strike for 1.2 and 0.25 km, respectively (Figs. 2 and 3). The east and west sides of North Slaughter Canyon are located 0.7–1.5 km apart along depositional and structural strike, and provide sub-vertical sections of faults and fractures A′–E (Fig. 2). The location, orientation (strike/dip) and overall structural similarities of faults/fractures A′, A, and E allows correlation across canyon with a high degree of confidence. In contrast, there is only one major fault trace on the west side of the canyon that is equivalent to fault traces B–D on the east. As it cannot be unambiguously correlated with any of the faults on the east, the single structure on the west is labelled B/D. The minor faults A″ and E′ are not correlated across canyon due to the absence of a counterpart on the east side of the canyon.

5.1. Conjugate faults A and B

On the west side of North Slaughter Canyon, fault A consists of two segments linked across a restraining bend (Fig. 5A). The fault has breached a growth fold between surfaces 11–16, and tips-out below a growth monocline bounded between surfaces 16–19. A body of stratiform breccia is found within the breached monocline. To the east, fault A comprises three linked segments (Fig. 5B). The lower segment tips-out below a growth monocline bounded between surfaces 2 and 4. The middle and upper segments

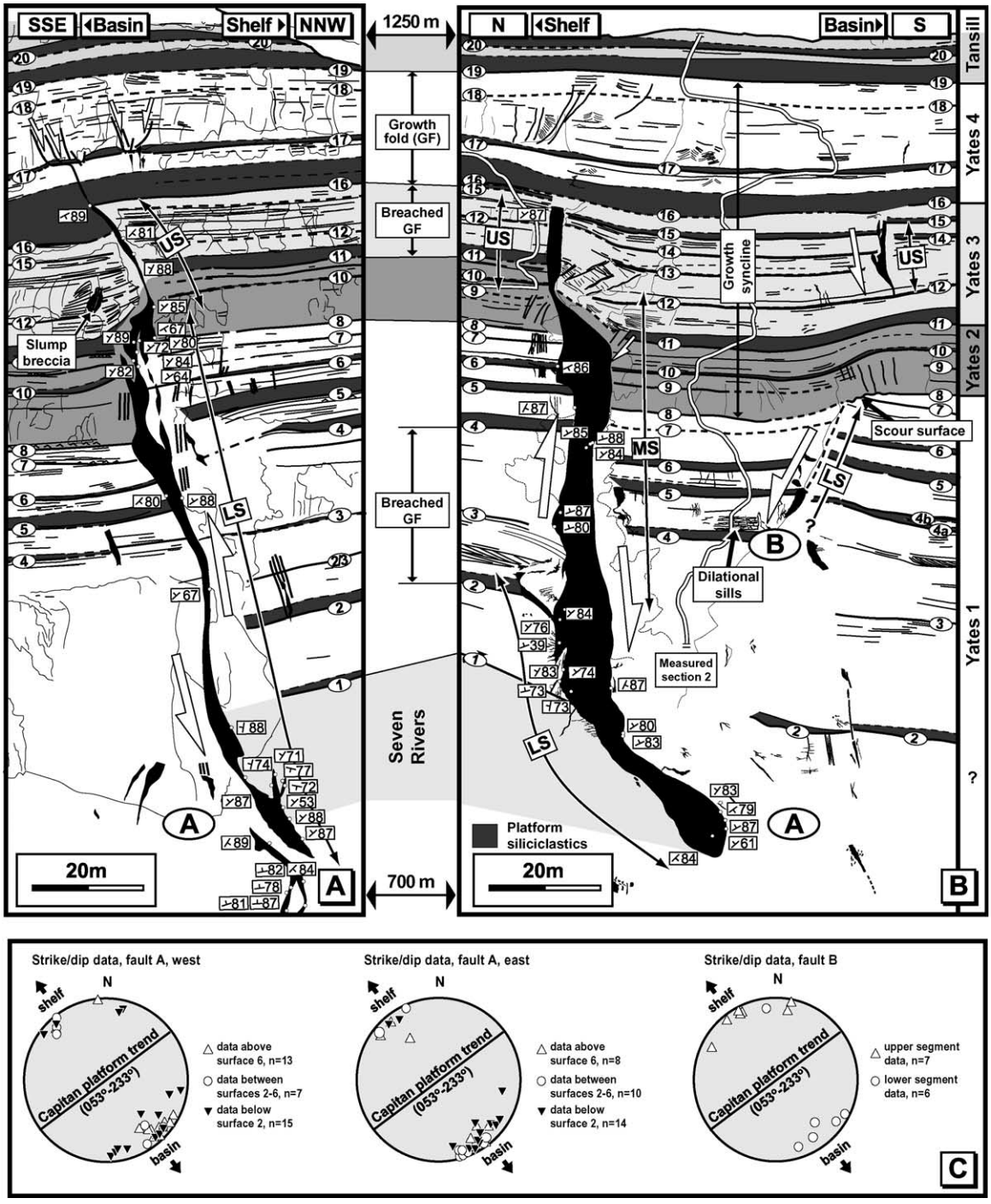

Fig. 5. (A, B) Line drawings summarising the outcrop appearance and relationships of fault zones A and B to platform stratigraphy; LS, lower segment; US, upper segment. The faults localised early dissolution, resulting in development of elongate palaeocaverns along them (shown in black). (C) Structural data. Note the apparent reverse fault geometry.

are linked across a restraining bend. A breached growth monocline is developed between surfaces 11 and 16. A small reverse fault cuts surface 11. Siliciclastics mantling surface 11 pinch out against this reverse fault (Fig. 5B). Approximately 300% growth is observed in strata bounded between surfaces 15 and 16 across the upper segment of fault A on the east. Surface 16 is not breached by the fault. A growth monocline bounded between surfaces 16 and 19 overlies the fault tip. On both sides of the canyon, the outcrop patterns and dip data indicate a reverse sense of displacement across fault A (Fig. 5C). The maximum measurable displacement is 24 m (Fig. 4B).

Fault B on the east side of North Slaughter Canyon consists of two dip-separated segments (Fig. 5B). The lower

segment tips-out abruptly at surface 8, which has the form of erosional scour within the footwall block. A network of extensional sills is developed within the immediate hanging wall of the lower segment. A growth monocline is developed over the tip of the lower segment between surfaces 8 and 18. There is a thickness difference of ca. 5 m across the monocline. The upper B segment cuts the growth monocline between surfaces 12 and 15. Strata between surfaces 15 and 16 thicken abruptly across the upper segment. Outcrop patterns and structural measurements indicate a normal orientation of the lower fault B segment. In contrast, the upper segment appears reverse (Fig. 5C).

5.1.1. Interpretation

Fault A shows little variation in displacement, dimensions and structure across canyon, a distance of 700–1250 m (Figs. 2 and 5). This pattern is interpreted to indicate that both exposures of fault A are located close to the fault centre (Fig. 6A). One important across-canyon difference, however, is that the lower A segment and related growth fold on the east are not developed on the west. This pattern is taken to indicate that the fault did not extend laterally across the canyon during deposition of strata 2–4 (Fig. 7B). Distribution of growth strata along the fault traces suggests that following a period of quiescence during the deposition of strata 4–7 the fault started to grow first on the west side of the canyon (Fig. 7C). During the deposition of the Y3-Tansill HFSs, the structural evolution of fault A appears to have been virtually identical across canyon (Fig. 7D–F).

The scour horizon in the footwall of the lower segment of fault B is considered to indicate that the fault broke surface 8 when it formed the top of the platform (Fig. 7C). Surface 8 represents the 4th-order Yates 1/Yates 2 HFS boundary, and is considered to have been associated with prolonged exposure. The erosional scour is thus interpreted to represent a degraded fault scarp, which disturbed the exposed top of the Capitan platform during lowstand associated with this major HFS boundary.

5.1.2. Growth folding and segment linkage

A shelfward-dipping growth monocline is developed over the tip of the lower segment of fault B, and resulted from 5 m of differential subsidence during deposition of strata 8–16. The upper fault B segment is dip-separated from the lower segment, and is interpreted to have grown in response to this differential subsidence (Fig. 6D and E). No upward propagation of the lower B segment however appears to have been associated with the growth folding. So, at least 5 m of movement appears to have occurred across the lower B segment *without vertical propagation of its upper tip*. Sills in the hanging wall of fault B (Fig. 5B) may indicate dilatation associated with this 'non-propagation' differential subsidence.

Fault A tips-out at, and very close to, surface 16. A basinward-facing growth fold is developed over its tip between surfaces 16–19, and has originated from at least 7.5 m of differential subsidence, resulting in 19% increase in thickness of these growth strata (Fig. 4A and B). As with the lower B segment, no vertical propagation of the fault tip appears to have been associated with this growth differential subsidence. The evidence for contemporaneous growth of the upper segments of faults A and B, and their structural similarity, lead us to anticipate that the upper fault A segment evolved from a primarily dip-separated segment similar to the upper segment of fault B. It is considered that linkage of the upper and lower segments of fault A may have facilitated differential subsidence and growth folding of strata 16–19 *without extending the fault length by means of vertical propagation of its upper tip* (Fig. 6F). Sandstone covering surface 16 might have acted as a stress absorber, and could have helped to accommodate the final stage of growth differential subsidence across fault A without faulting of strata 16–19.

5.2. Fault C

Fault C appears to be sub-vertical, and reveals both basinward and shelfward sense of throw (Fig. 7A and B). Strata bounded between surfaces 3 and 4b thicken by ca. 7 m on the basinward side of fault ca. This indicates that the fault was down-throwing basinward during deposition of strata 3–4b. In contrast, strata bounded between surfaces 4b–5 thicken shelfward. This indicates that the movement on the fault was reversed during deposition of surfaces 4b–5, after which time the movement of the fault ceased, as evidenced by the continuity of strata overlying surface 5.

5.3. Fault D

D is a segmented normal fault (Fig. 7A and B). It consists of two distinct segments offset across a fractured, 3 m wide, restraining off-step (Fig. 7A). Approximately 9 m of throw can be measured across fault D. No growth strata appear to be associated with this fault, indicating that it grew at depth and had no influence on the depositional surface. It is interpreted to have grown during deposition of strata younger than surface 11. The lack of growth strata, however, prevents the establishment of a more accurate timing. Palaeocaverns developed along the fault contain deposits derived from the Capitan platform top. The lithology, early diagenesis (marine cementation, dolomitisation), and Permian age of fauna within the palaeocavern fills provide unambiguous evidence of Capitanian age of this fault (Fig. 7C).

5.4. Fault E

On the west, fault E consists of two segments linked across a restraining bend. It tips-out abruptly within siliciclastic strata deposited above surface 16 (Fig. 8A). A breached growth monocline bounded by surfaces 10–12 is

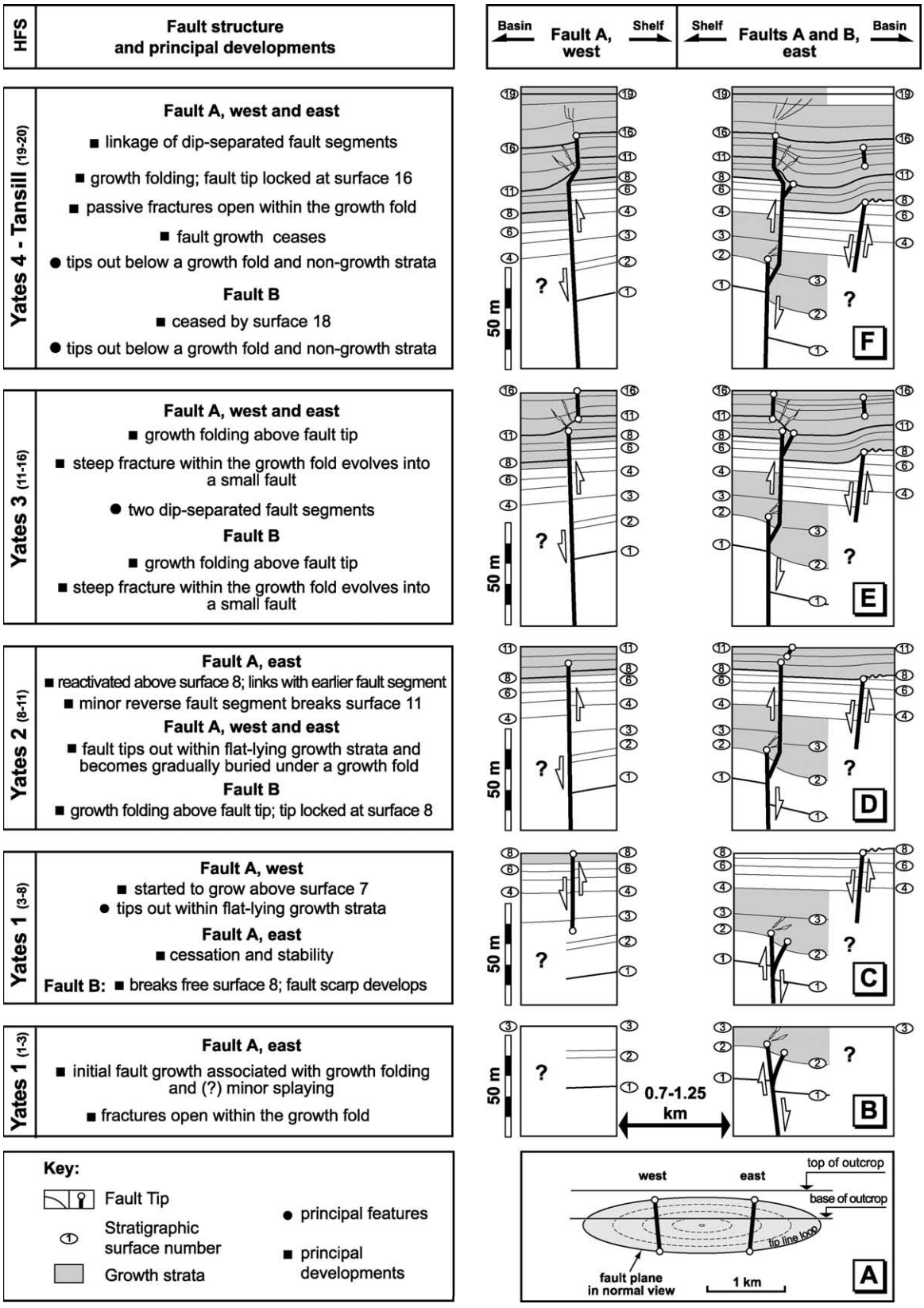

Fig. 6. Spatial and temporal evolution of faults A and B. (A) Similarity in structure and scale of fault A across canyon (i.e. 0.7–1.25 km along-strike) is interpreted to indicate that the two cross-sectional outcrops of the fault are located in a similar position with respect to the fault centre. (B)–(F). Models illustrating the growth of faults A and B in relation to platform deposition. The present-day structural configuration of the faults is shown in Fig. 5, and approximates the stage F here.

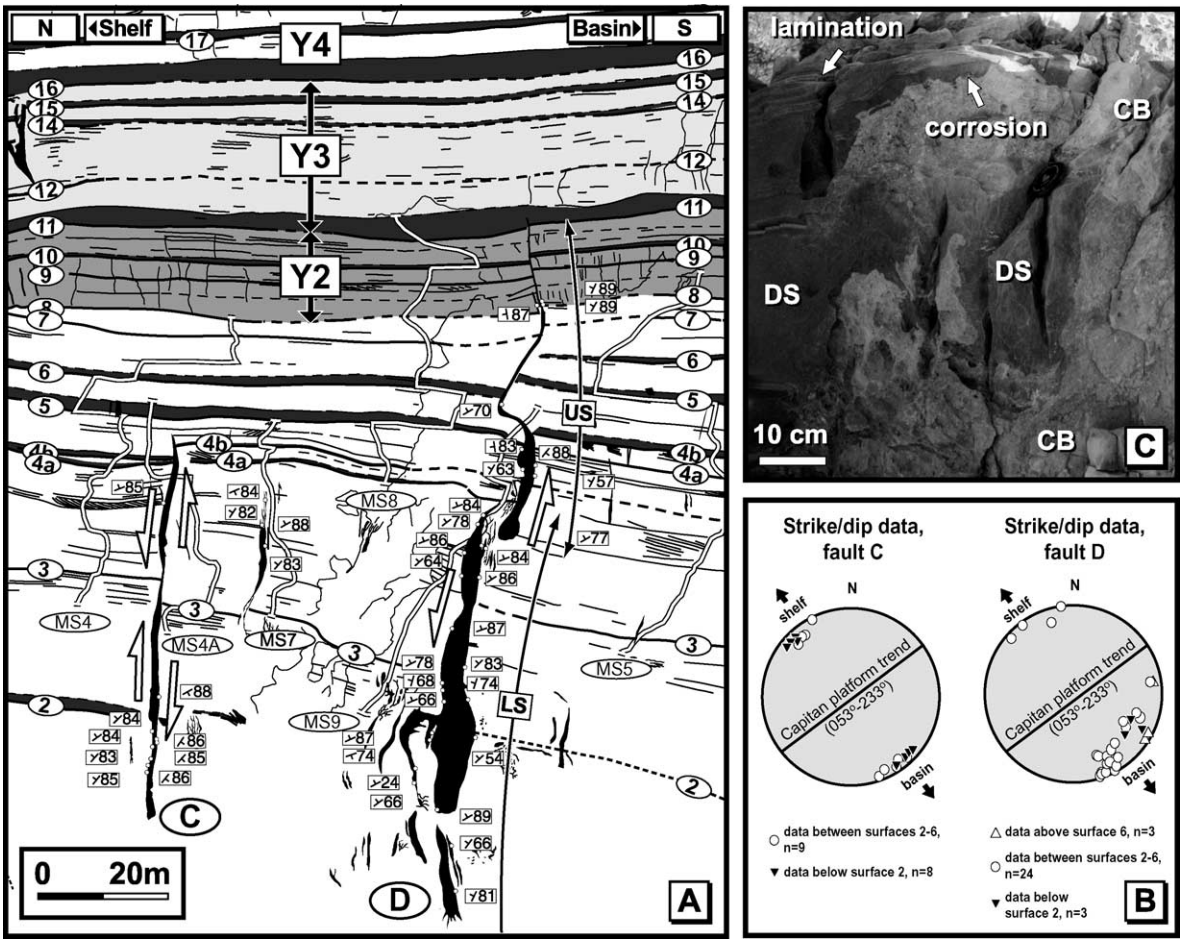

Fig. 7. (A) Line drawing of fault zones C and D on the east side of North Slaughter Canyon. Fault C has accumulated ca. 7 m of growth on its basinward side during deposition of strata 3–4b. This sense of displacement was reversed during deposition of units 4b–5. In contrast, fault D never reached or affected the free surface. LS, lower segment; US, upper segment. (B) Structural data. Fault C is sub-vertical, while fault D dips shelfward at ca. 80°. These dips, and the inversion of fault C, are interpreted to result from rotation of the faults basinward, as a consequence of syndepositional down-to-basin tilting of the Capitan platform. (C) Platform-derived sediments fill palaeocaverns developed along fault D, and confirm its Capitanian age (DS, dolomitic sandstone; CB, carbonate breccia; Koša et al. (2003)).

developed along the fault trace. The fault appears to link downward into a splay of sediment-filled passive fissures within the Capitan reef (Fig. 8A). On the east, fault E also consists of two segments linked across a restraining bend. However, on the east it tips-out below a growth monocline bounded between surfaces 8–16 (Fig. 8B). Platform strata lap onto the shelfward-dipping flank of the monocline. A passive dilatational fissure cuts through the growth fold. It tips-out below surface 15, and is filled by siliciclastics that connect to, and apparently originated from, siliciclastics mantling this surface.

5.4.1. Interpretation

The stratigraphic position and structural style of the upper tip of fault E is significantly different on either side of North Slaughter Canyon, i.e. some 1.2 km along-strike (Figs. 2 and 8). The patterns of the along-strike variability are interpreted to indicate that cross-section of fault E on the east is located further from the fault centre compared to the exposure of the fault on the west.

A series of tensional fissures within the Capitan reef appears to have controlled the location of fault E on the west (Fig. 8A). Growth folding of strata 10–12 indicates that the fault was active during their deposition (Fig. 8A). The isopachous nature of strata 12–16 in turn indicates an episode of quiescence, which was followed by a brief reactivation of the fault during the deposition of siliciclastics mantling surface 16, which are seen to thicken across the fault. In contrast, on the east fault E is interpreted to have grown in a shallow subsurface during the deposition of strata 8–16. The depositional onlap of strata onto the shelfward flank of the growth monocline suggests that as it developed, the fold has induced some 2 m of topographic relief on the contemporaneous sea floor (Fig. 8B; Hunt et al., 2002). On either side of the canyon the fault is considered to have ceased by the end of deposition of siliciclastics above surface 16.

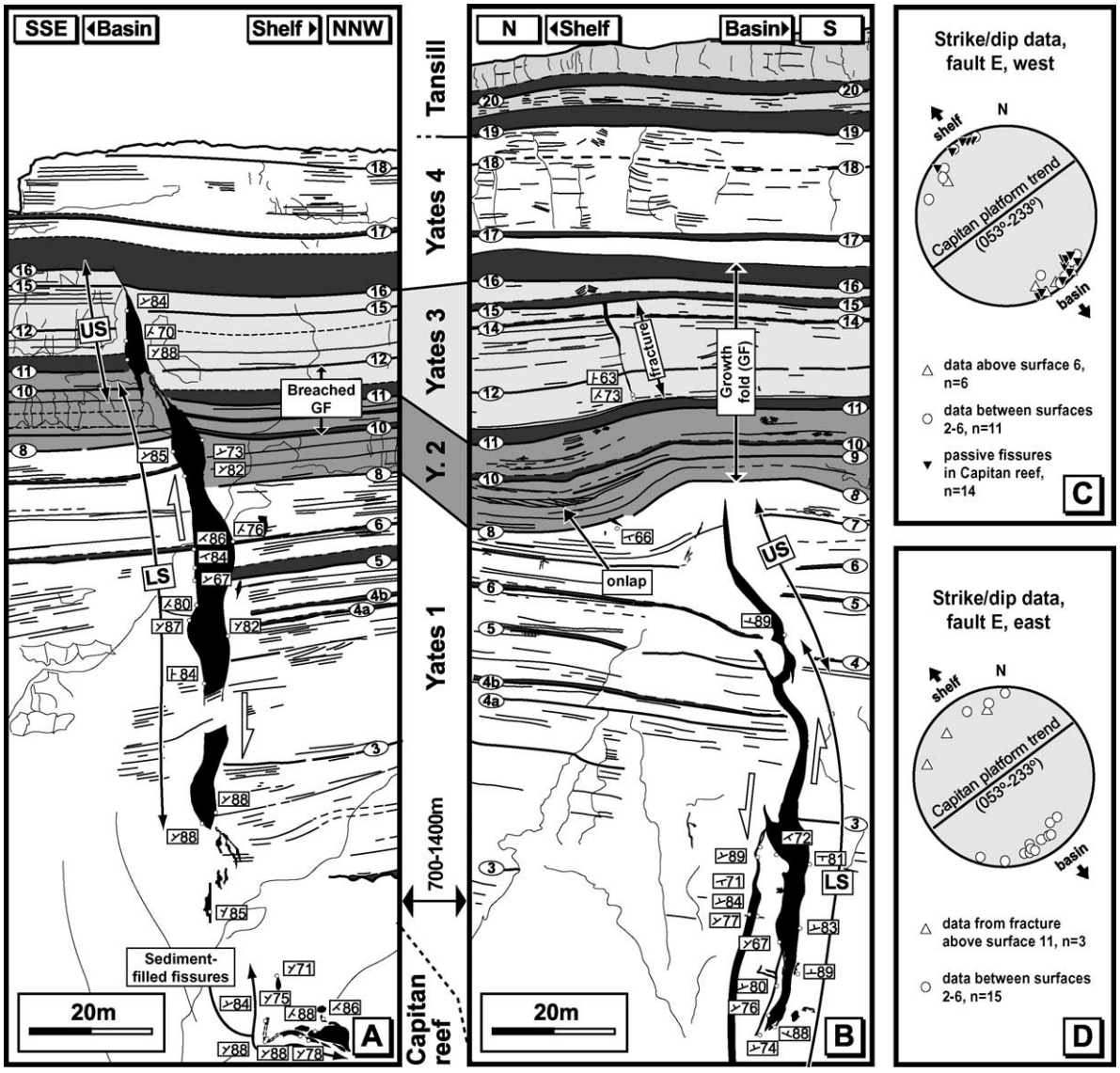

Fig. 8. (A and B) Comparison of structural characteristics of fault E on the west (A) and east (B) sides of North Slaughter Canyon. LS, lower segment; MS, middle segment; US, upper segment. (C and D) Stereonets showing orientation (as poles) of karst-modified fault segments and fractures.

5.5. Fault/fracture A′

Fault A′ on the west (Fig. 9A) is equivalent to a passive fissure on the east, 700–1000 m along-strike (Figs. 2 and 9B). A′ on the west is composed of several segments that tip-out upward into a fault splay below a monocline (Fig. 9A). Carbonate-rich deposits filling the lower part of the fault zone under surface 1 are pervasively fractured and partly reworked into cataclastic spar breccia. The fault throws toward the basin. Outcrop patterns and dip data indicate a reverse sense of displacement. Two branches in the upper part of the fault bound a small collapse trough. A shelfward sense of displacement is observed across the uppermost part of the SSE branch of fault A′ (Fig. 9A).

A sedimentary breccia rests on surface 2b, and erodes into the footwall of fault A′ on the west side of the canyon. Clasts as large as 20 cm across are found near to the fault trace. Clast size and frequency decrease with distance from the fault. A similar breccia rests on surface 2 on the east side of the canyon (Fig. 9).

On the east, carbonate and siliciclastic sediments fill the passive fissure A′ (Fig. 9B). Carbonate platform strata overlying the fissure-filing deposits show patterns of soft-sediment deformation, and have partly collapsed into the fissure. Strata between surfaces 2 and 3 are fractured and partly brecciated, and a narrow syncline is evident at surface 3 over the fissure. Outcrop patterns and dip data indicate a shelfward dip of the fissure (Fig. 9B).

5.5.1. Interpretation

The along-strike variability in structure of fault/fracture A′ is interpreted to indicate that the low-displacement fault on the west is located near to a lateral termination of a larger-scale fault zone (Fig. 10A). Sedimentary fill within

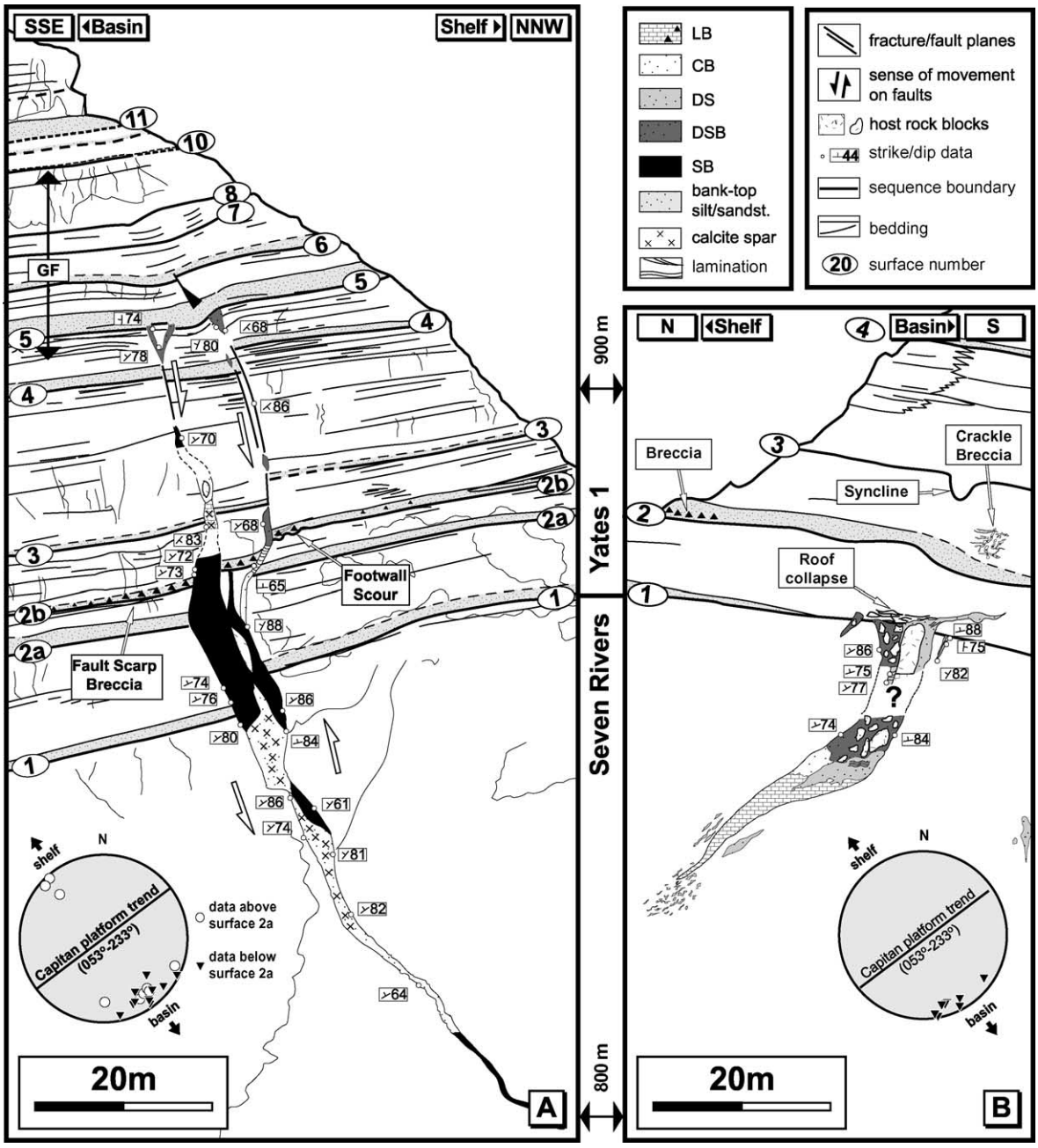

Fig. 9. Line drawing of fault/fracture A′ on the west (A) and east (B) side of North Slaughter Canyon. On the east, A′ is solely expressed as a sediment-filled passive fissure. In contrast, on the west it has evolved into a reverse fault. The reverse sense of displacement, and the shelfward dip of A′ are interpreted to have resulted from basinward rotation in course of down-to-basin tilting of the Capitan platform. LB, limestone breccia; MSB, microspar breccia; SB, spar breccia; DS, DSB, beige dolomitic silt/sandstone and associated breccia; CB, carbonate-rich breccia; GF, fault propagation growth fold. Detailed description of the palaeocavern-filling lithologies is in Koša et al. (2003).

the lower part of fault/fracture A′ on either side of North Slaughter Canyon under surface 1 (Fig. 9) indicates that a sediment-filled passive fissure analogous to A′ on the east localised the development of fault A′ on the west (Fig. 10B). Cataclastic reworking of sediments filling fault A′ on the west (Fig. 9A) is interpreted to have resulted from linkage of the precursor fissure into a fault (Fig. 10C). Erosional scour within the immediate footwall of the fault at surface 2b, and breccia deposited over it, are interpreted to represent a degraded fault scarp. This feature is taken to indicate that fault A′ breached the platform top during deposition of siliciclastics mantling surface 2b (Fig. 10C). Breccia covering surface 2 on the east (Fig. 9B) was probably derived form the same source. Thickness and facies changes across fault A′ indicate that it was inactive during the deposition of strata 2b–5, and was re-activated afterwards to form the composite structure presently observed (Fig. 10D).

On the east, the collapse, brecciation and folding of strata overlying the A′ fissure is thought to have occurred in response to compaction of the siliciclastic-dominated fill of the fissure. It is also possible that the fissure was reactivated at depth during the deposition of strata bounded between surfaces 3–4 (Figs. 9B and 10D).

5.6. Conjugate faults Z1 and Z2

Z1 and Z2 are closely spaced, segmented, antithetic faults (Fig. 11A–C). Fault Z1 consists of three segments (Fig. 11A and B), whereby the lower segment is reverse and tips-out below a growth monocline bounded between surfaces 7 and 16 (Fig. 11C). The monocline between surfaces 7 and 16 is breached by the normal middle Z1 segment (Fig. 11A–C). No thickness change is observed across the middle Z1 segment. The fault segment widens upward and is filled by chaotic collapse breccia with a red-stained siliciclastic matrix. A growth monocline is developed over the tip of the middle Z1 segment between surfaces 16 and 20. The monocline is cut in its lower part by the upper Z1 segment. The middle and upper Z1 segments are laterally separated across a restraining off-step. The upper Z1 segment has a reverse sense of displacement (Fig. 11C). Internally, it consists of two smaller, upwardly opening segments linked across a restraining bend (Fig. 11B and C). These are filled by red sandstone similar to sandstones overlying surfaces 17 and 18, below which these upwardly opening segments tip out.

Fault Z2 has a normal sense of displacement, and consists of two segments separated across a restraining off-step (Fig. 11A–C).

5.6.1. Interpretation

The structural development of faults Z1 and Z2 is illustrated in Fig. 12. The lower segment of fault Z1 and fault Z2 represent conjugate faults, whereas Z1 is steep reverse, and Z2 is a steeply dipping normal fault (Fig. 11C). Growth strata indicate that approximately 15 m of throw took place across the lower Z1 segment during deposition of strata bounded between surfaces 2–5, followed by a short break (Figs. 11D and 12A). Growth folding of strata 7–16 over the tip of the lower Z1 segment indicates reactivation of the fault during their deposition (Figs. 11A, B, D and 12B, C). Fault Z2 is interpreted to have grown during the deposition of strata bounded between surfaces 7 and 16, exerting no influence on the depositional topography (Fig. 12C). The growth of both faults is interpreted to have then ceased, followed by development of the middle and upper segments of Z1 (Fig. 12C and D).

5.6.2. Growth folding and segment linkage

The middle and upper segments of fault Z1 well illustrate the relationships between folding, fracturing and fault-segment linkage (Fig. 12E–H). They open upwards, and contain sedimentary fills that are lithologically similar to platform sediments overlying their upper tips (Fig. 12H). The middle segment of fault Z1 is filled by chaotic collapse breccia with a red-stained siliciclastic matrix that has apparently originated from siliciclastics deposited over surface 16. No discrete thickening of these siliciclastic strata is observed across the middle Z1 segment. The fault segment is therefore, considered to have evolved from an upwardly opening extensional fracture formed in the growth monocline above the tip of the lower Z1 segment (Fig. 12C–G). It appears that *propagation downward* of the middle segment has lead to its linkage with the lower segment, in a manner similar to that inferred for the previously described linkage of the upper and middle segments of fault A (Fig. 6E and F).

This siliciclastic fill of the upper Z1 segment appears to have been derived from siliciclastics mantling surfaces 17 and 18, below which the two segments of the upper Z1 segment tip out (Fig. 12H). On the basis of the fill, morphology, and the lack of discrete across-fault thickness changes, the upper Z1 segment is interpreted to have evolved from a pair of steep, shelfward-dipping extensional fractures (Fig. 12E–G). These are thought to have originated in response to growth folding of strata 16–18 over the tip of the middle Z1 segment. This growth folding is also taken to be responsible for their mutual linkage and evolution into the upper Z1 segment (Fig. 12E and F).

6. Dynamic growth and linkage of syndepositional faults and fractures

The structural characteristics of syndepositional faults and fractures in North Slaughter Canyon are observed to vary vertically and laterally. This heterogeneity is taken to approximate temporal and spatial variations in the structural evolution of the faults and fractures. The following features are identified as major controls on structural variability of syndepositional faults: (i) incremental growth, (ii) temporal changes in the sense of movement, (iii) growth by linkage of vertically separated segments, (iv) interaction with pre-existing fractures, and (v) variations in differential subsidence and platform-aggradation rates. Some of these are discussed in more detail below.

6.1. Temporal changes in sense of fault movement

Syndepositional faults in the Capitan platform are very steep, with a mean dip greater than 75°. Faults that downthrow towards the shelf mostly have a normal sense of displacement, and tend to dip at shallower angles in comparison to faults throwing toward the basin (e.g. compare faults B, D, E, Z2 and A, C, A′, Z1; Figs. 5C, 7B, 8C, D, 9 and 11C). This pattern is also observed in pairs of conjugate faults (e.g. A–B, lower Z1 segment–Z2; Figs. 5B and 11C). Exceptions are small fault segments within shelfward-dipping growth monoclines (e.g. upper B

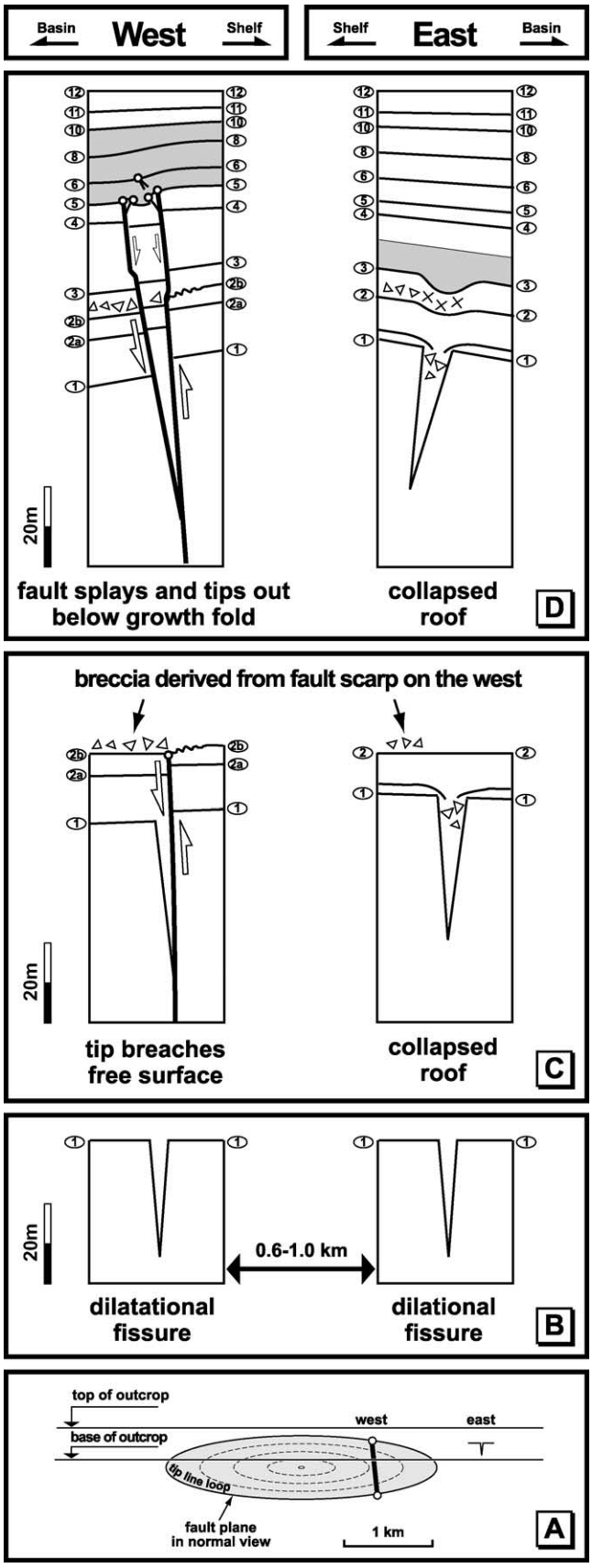

Fig. 10. Spatial and temporal evolution of fault A′. (A) Along-strike variability observed across North Slaughter Canyon indicates that fault trace on the west is positioned close to a lateral termination of a fault that had evolved from a pre-existing passive fissure. On the east, the fissure has not evolved into fault. (B)–(D) Schematic reconstruction of the structural development of fault and fracture zone A′. See text for details. Grey colour indicates growth strata.

segment; Fig. 5B). Basinward-throwing faults are sub-vertical, and most of them are reverse (A, A′, lower Z1 segment; Figs. 5C, 9 and 11C). Some of the primarily basinward-throwing faults have changed the sense of movement as they developed, thus converting themselves into shelfward-throwing faults (C, A′, lower Z1 segment; Figs. 7A, 9A and 11B).

Previous studies of geopetal and bedding data have demonstrated that strata within the outer part of the Capitan platform were progressively tilted down to basin by at least 10° as the platform developed (Saller, 1996; Harwood and Kendall, 1999; Longley, 1999; Hunt et al., 2002). Differential compaction of fine basinal siliciclastics, over which the platform prograded, is thought responsible for the tilting. In accordance with this interpretation, syndepositional faults within the platform strata are interpreted here to have been rotated in a basinward direction as the platform tilted down to basin. The sense of displacement on primarily basinward-dipping faults is thus thought to have changed from normal to reverse as the faults were rotated past the vertical, turning themselves into shelfward-dipping faults. As a result, some of the faults appear to have a reverse sense of displacement (e.g. A, A′, lower Z1 segment; Figs. 5, 9A and 11). Some of the faults, however, had their movement inverted, and changed into shelfward-throwing normal faults as they passed the vertical (e.g. C, upper segment 1 of A′; Figs. 7 and 9A).

6.2. Segment linkage and interaction with inherited fractures

Two types of passive extensional fissures appear to have been significant for the growth of syndepositional faults: (i) fissures within the Capitan reef and immediate back-reef strata and (ii) fractures associated with growth folds within the platform strata.

Extensional fissures within the Capitan reef and immediate back-reef strata appear to have localised growth of faults E and A′ (Figs. 8A and 10). Fissures are interpreted to have developed near to the platform margin in response to compaction-induced instability and break-up of the steep-sloped Capitan reef (Fig. 13A). Such fissures are a common feature of reef-rimmed platform margins. Fissures breaking up the Capitan platform margin are considered to have later localised the foundation of syndepositional faults within platform strata that prograded over the margin (Fig. 13B).

Syndepositional faults in the Capitan platform commonly tipped out below growth monoclines. The growth folds are typically cut by upwardly opening and diverging extensional fractures (e.g. E; Fig. 8B). In some cases,

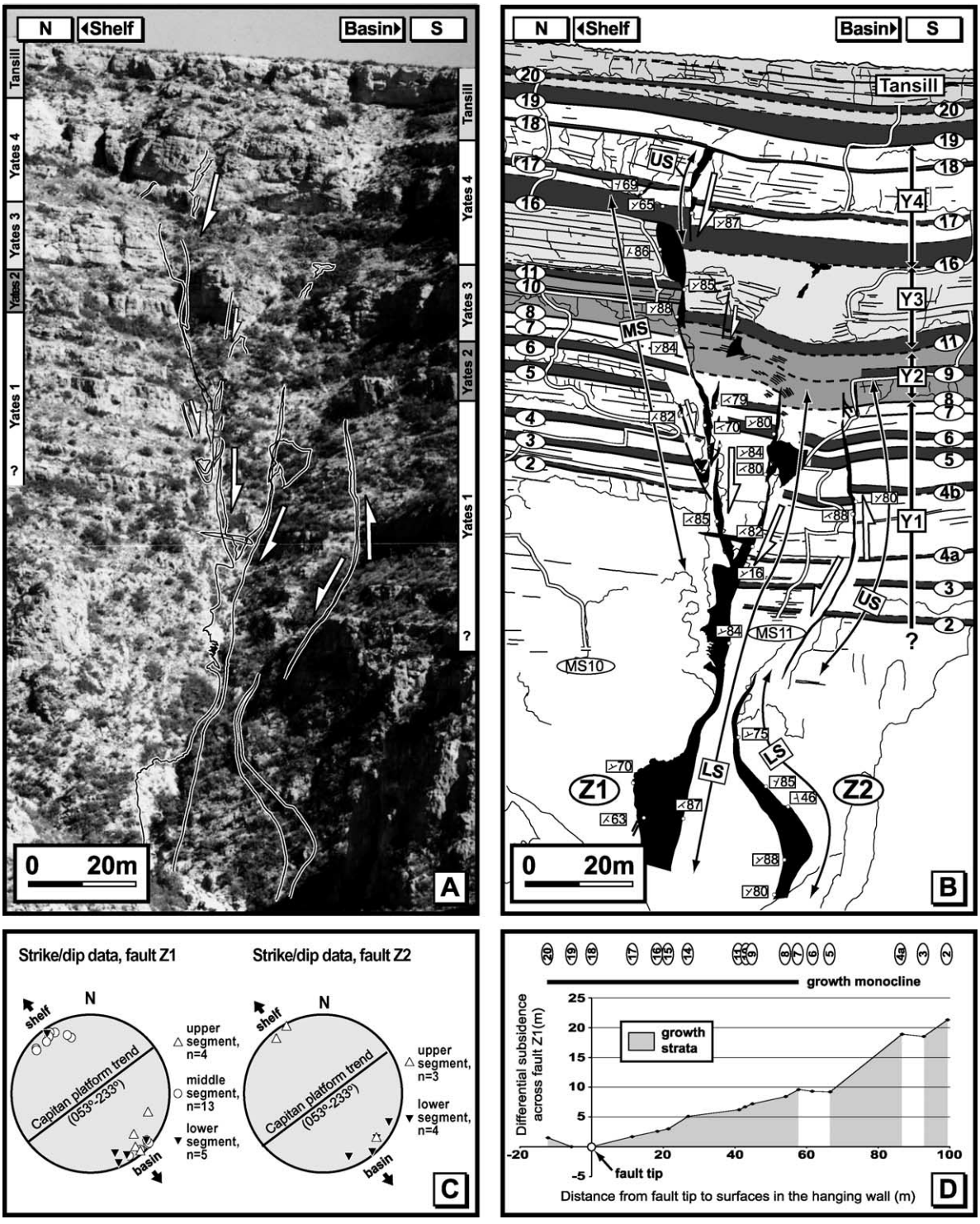

Fig. 11. Photograph (A) and line drawing (B) of faults Z1 and Z2. LS, lowers segment; MS, middle segment; US, upper segment. (C) Structural data. Reverse orientation of lower Z1 segment is interpreted to have originated from rotation as the fault grew due to down-to-basin tilting of the Capitan platform, in a manner similar to faults C and A′. (D) Differential displacement/distance curve of fault Z1. Distribution of growth strata is indicated.

steeply dipping fractures located at the top of the growth monoclines appear to have evolved into separate fault segments (e.g. B, upper Z1 segment; Figs. 5, 11 and 12C–H). Some of these segments appear to have linked into underlying fault segments to form single fault traces (e.g. A, middle Z1 segment; Figs. 5, 11 and 12C–H). The patterns of the upper A and the middle and upper Z1 segments are considered to indicate that linkage of the initially isolated segments occurred through *downward* propagation of the higher segments (Figs. 6F, 12 and 13C, D).

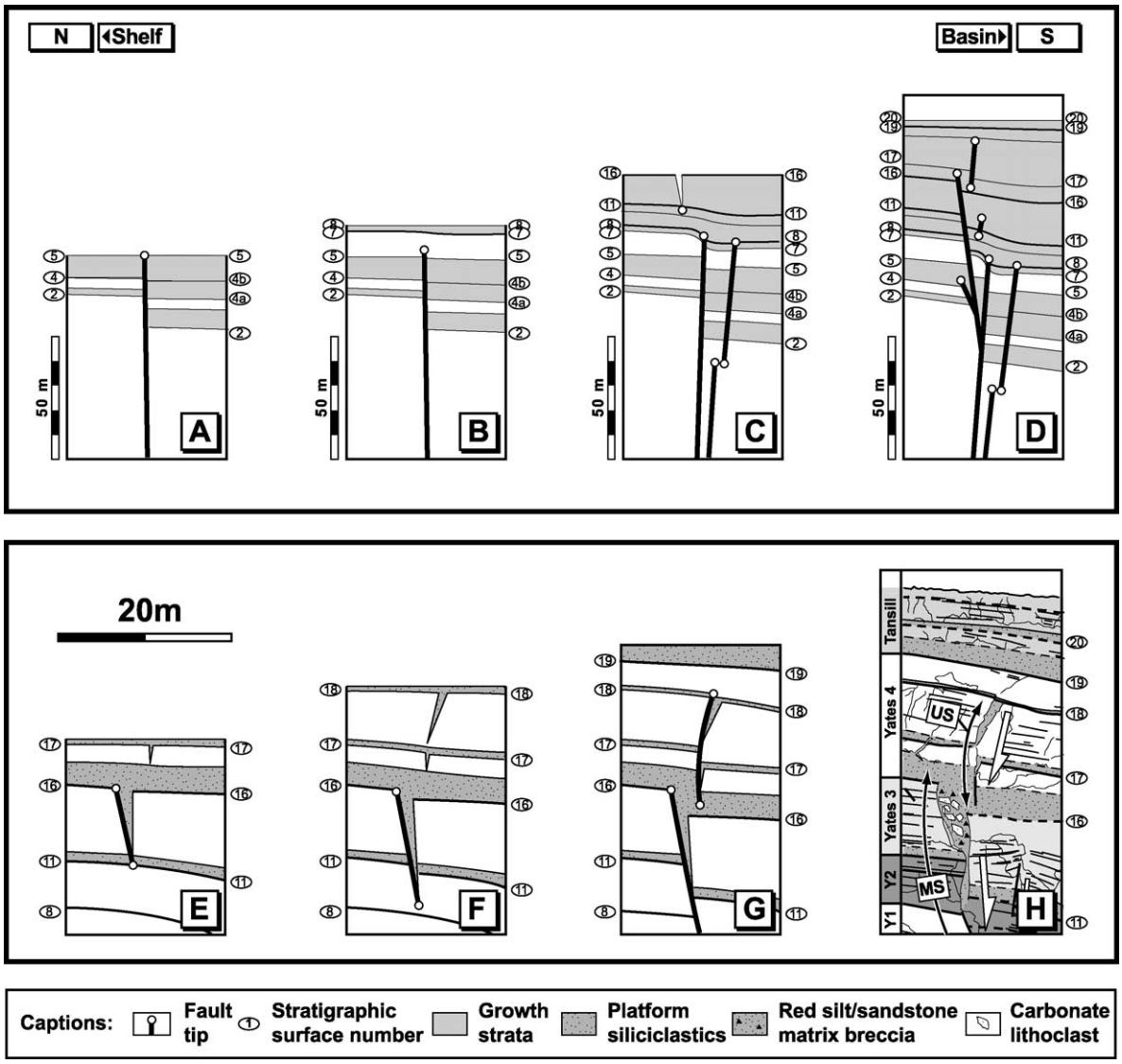

Fig. 12. (A)–(D) Idealised cross-sections illustrating the interpreted temporal structural evolution of faults Z1 and Z2. (E)–(G) Models showing in detail how the middle and upper segments of fault Z1 are interpreted to have evolved from extensional fractures formed during growth folding. (H) Outcrop map of structure shown schematically in G. MS: middle segment. US: upper segment. See text for details.

Small reverse faults and fault splays are commonly found within growth folds (e.g. A, B, Z1; Figs. 5A and 11). These reverse faults are interpreted to have served to facilitate mass transfer needed to accommodate differential subsidence within the monoclines (Horsfield, 1977; Withjack et al., 1990; Hardy and McClay, 1999). Fractures within growth folds with dips antithetic to the fold-forcing faults were inherently prone to evolve into the reverse faults, as is shown schematically in Fig. 13C and D.

6.3. Fault-related growth folding

Growth monoclines developed within strata overlying the upper tips of fault A and the lower segment of fault B are shown above to have grown through at least 7.5 and 5 m of differential subsidence, respectively. This differential subsidence took place *without any upward propagation of the underlying fault tips* (Fig. 6D–F). Linkage of the previously separated middle and upper fault segments at depth is interpreted to have driven the 'non-propagation' folding above fault A while its upper tip was locked at surface 16 (Fig. 6F). Unfortunately, the outcrop does not permit to observe whether the same mechanism can be applied to the lower B segment (Fig. 5). Similar patterns are observed associated with fault Z1, where strata bounded between surfaces 16–18 have been folded over the tip of the downward-propagating middle Z1 segment (Fig. 11). No upward propagation of the middle Z1 segment occurred in course of the growth folding of strata 16–18 (Fig. 12E and F). The patterns of growth folds associated with faults A, B and Z1 thus show that significant growth folding has occurred across faults whose upper tips were temporarily

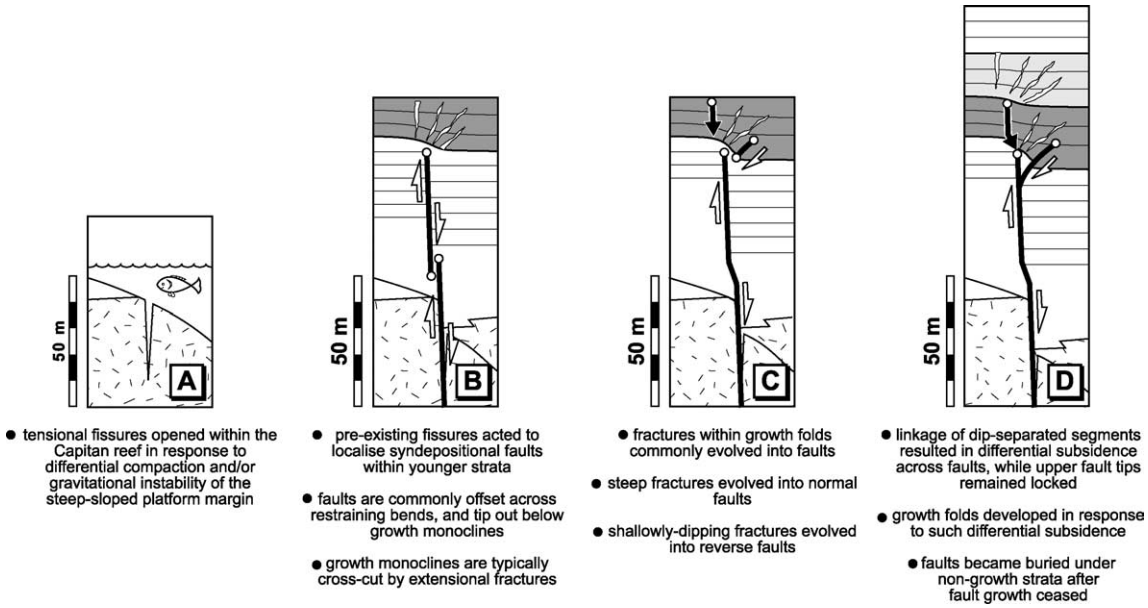

Fig. 13. Model showing the importance of inherited fractures and segment linkage for fault growth.

locked while more displacement accumulated towards the fault centres. Slip events limited to patches on the pre-existing fault surfaces, downward propagation of the fold-forcing fault segments, and linkage of previously unconnected segments at depth, are inferred to have facilitated the 'non-propagation' differential subsidence (Fig. 13). Also, siliciclastics mantling surface 16 might have acted as a stress absorber, providing a mechanostratigraphic barrier to vertical propagation of the A and middle Z1 fault tips.

7. Fault propagation, platform aggradation, and fault structure

Structural and stratigraphic observations described above demonstrate that faults in the Capitan platform grew incrementally, so that their differential subsidence rates varied through time. Rates of platform aggradation also varied though time: relatively rapid deposition of thick carbonate strata during highstands alternated with comparably retarded deposition of thin sheets of siliciclastics during lowstands. The rates of highstand deposition thus greatly exceeded those of lowstand deposition. Locally, non-deposition and/or erosion took place during lowstands. As a consequence, growth-differential-subsidence/platform-aggradation ratios would have varied through time.

7.1. Differential subsidence at free surface

Faults breaking-free surface provides an opportunity to estimate the local fault-slip rates at the time of surface breakage. If slip rates at free surface exceed rates of deposition, fault scarps develop. The rare occurrence and the low topography of palaeoscarps associated with faults in the Capitan platform (e.g. B, A′; Figs. 5B and 9A) indicate that differential subsidence at free surface rarely exceeded the rates of platform aggradation. Degraded fault scarps are exclusively found associated with sequence boundaries, and appear to have developed during periods of limited lowstand deposition. It would thus appear that highstand sedimentation rates were always high enough to keep pace with, or outpace, differential subsidence across faults disrupting the free surface. These patterns are taken to indicate that differential subsidence rates at the free surface never exceeded rates of platform-aggradation during sea-level highstands, i.e. 0.053–0.336 m/ka (Hunt et al., 2002).

Below are examples of growth-differential-subsidence/-platform-aggradation ratios (*GDS/A*) calculated for faults A and Z1. These are followed by discussion of how variations in the *GDS/A* ratios influenced the structure and stratigraphy associated with fault tips.

7.2. GDS/A ratios, fault A

Fault A tips-out upward below surface 16. Distribution of growth strata along fault A shows that the fault was active during the deposition of strata 2–4 and 8–19, and permits to establish the *GDS/A* ratios for various growth-fault-propagation events. A mean *GDS/A* ratio can be calculated for the intermittent growth of fault A between surfaces 2 and 16, during which strata 2–18 were deposited: $GDS_{(2-16)}/A_{(2-19)} = 154/195.5 = 0.79$. Surface 8 represents the highest possible point at which the fault tip could have occurred at the beginning of the faulting event associated with growth of strata 8–19 (Fig. 4C). The *GDS/A* ratio for this period of fault evolution can thus be derived by dividing the hanging wall distance between surface 8 and the fault tip at surface 16 by the hanging wall thickness of strata 8–19:

$GDS_{(8-16)}/A_{(8-19)} = 72.8/113.1 = 0.64$. The pinch-out of siliciclastics bounding surface 11 against the middle fault A segment shows that at this level the fault broke the free surface (Figs. 5B and 6D). The *GDS/A* ratio for propagation of the fault tip from the level of surface 11 to 16 can be derived by dividing the hanging wall distance between surface 11 and the fault tip at surface 16 by the hanging wall thickness of strata 11–19 deposited during this fault-growth event: $GDS_{(11-16)}/A_{(11-19)} = 47.6/87.9 = 0.54$.

7.3. GDS/A ratios, fault Z1

Distribution of growth strata along fault Z1 indicates that, with short breaks during the deposition of strata 3–4a and 5–7, the fault was active throughout the deposition of strata bounded between surfaces 2–20 (Fig. 11D). Following a break in fault growth during deposition of strata 5–7 (Fig. 11D), the fault tip is interpreted to have propagated from surface 5 to 8 as strata bounded by surfaces 7–16 were deposited (Fig. 12B and C). The upper Z1 segment tips-out upward at surface 18, and is overlain by growth-fold strata topped by surface 20 (Fig. 11A and B).

A mean *GDS/A* ratio of Z1 during propagation of fault tip from surface 2 to 18 can be established by dividing the hanging wall distance between surface 2 and the tip of the upper Z1 segment at surface 18 by the hanging wall thickness of strata bounded by surfaces 2–20: $GDS_{(2-18)}/A_{(2-20)} = 104.5/11.5 = 0.94$. Surface 7 represents the highest possible point at which the fault tip could have occurred at the beginning of the faulting event associated with growth of strata 7–16 (Fig. 12B–C). The *GDS/A* ratio for this period of fault evolution can thus be derived by dividing the hanging wall distance between surface 7 and the fault tip at surface 8 by the hanging wall thickness of strata 7–16: $GDS_{(7-8)}/A_{(7-16)} = 7/39.4 = 0.18$.

7.4. GDS/A ratio, fault structure and platform stratigraphy

Quantitative data show that the mean *minimum GDS/A ratios* for faults A and Z1 equal 0.79 and 0.94, respectively. Thus on average, differential subsidence rates appear to have been slightly lower than those of platform aggradation. This implies that fault tips would have been likely to be found close to depositional surface. This is consistent with the presence found along the fault traces of non-folded growth strata and with evidence for faults occasionally breaking the free surface (Figs. 6, 9 and 12). On the other hand, the *GDS/A ratios* calculated between successive fault tips during final stages of evolution of fault A and the lower Z1 segment are much lower than 1, and are consistent with the observation that the faults became buried under growth monoclines and, eventually, non-deformed strata. Quantitative data thus appear to be consistent with observations on the faults structure and platform stratigraphy.

Unfortunately, no reliable criteria could be established to quantify the *GDS/A* ratios for fault-growth events that have lead to the development of fault scarps found along faults A, B and A′ (Figs. 5 and 9). This is because erosional scour within footwall is difficult to be unambiguously correlated with contemporaneous deposits within hanging wall. It is certain, however, that *GDS/A* ratios for these fault-growth events would be greater than 1. All fault scarps that had originated during the slowdown in deposition during sea-level lowstands were eventually levelled by the accelerated highstand-carbonate deposition, at which point the *GDS/A* ratios would have equalled 1. The interplay between the rates of differential subsidence and platform aggradation, and its importance for fault-tip structure and stratigraphy is discussed in more detail below.

7.5. Morphology of upper fault tips

Four morphological types of upper fault tip can be identified on the basis of their relationships with depositional surfaces and association with growth strata. These are: (I) fault tips that broke free surface, (II) fault tips associated with non-folded growth strata, (III) fault tips buried below growth monoclines and (IV) buried tips of faults not associated with growth strata (Fig. 14). All faults recognised to date in the Capitan platform show one of the four types of upper termination. Below are some examples that best illustrate these fault-tip patterns.

7.5.1. Faults breaking free surface (type I tip)

For example, the erosional scour on top of the footwall block of the lower fault B segment is considered to represent a degraded fault scarp, and is taken to indicate that the fault broke the free depositional surface 8 (Figs. 5B and 6C). The upper termination of the lower fault B segment at surface 8 is therefore distinguished as a type I fault tip (Fig. 14A). Fault A′ is considered to have tipped out with a type I termination during exposure of surface 2b (Figs. 9A and 10C).

7.5.2. Faults associated with non-folded growth strata (type II tip)

The upper segments of faults A and B on the east side of North Slaughter Canyon tip out blindly within strata 15–16 (Fig. 5B). No erosional scours are, however, found at or above the broken surface 15, and thickening of strata is discrete across the shallowly buried fault scarps. Separations of surface 15 by these faults are therefore inferred to have occurred concurrently with deposition of overlying carbonate strata whose aggradation kept pace with, or outpaced, the growth of the fault scarps. Such structures are distinguished as type II fault tips (Fig. 14B).

7.5.3. Faults tipping out below growth folds (type III tip)

Fault E on the east side of North Slaughter Canyon tips-out upward below a growth monocline, and thus represents a typical example of fault with a type III termination (Figs. 8B

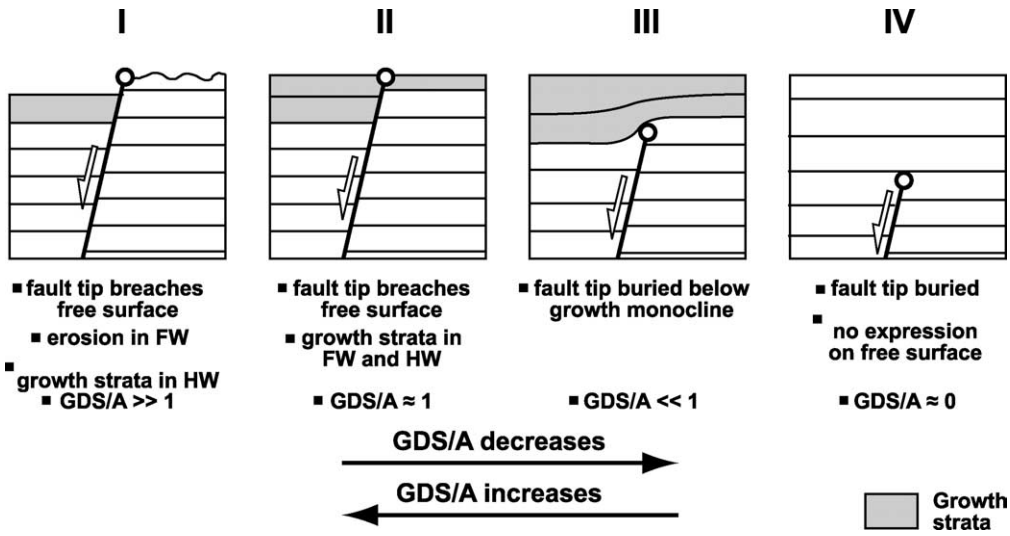

Fig. 14. Illustration of the role of interplay between growth differential subsidence (*GDS*) and platform aggradation (A) in controlling structures associated with upper fault tips. Four principal types of fault tips are identified, namely: I, degraded fault scarps; II, tips at free surface associated with growth strata; III, tips below growth folds; and IV, buried tips not associated with growth strata. The fault tips evolved from one type into another as the faults grew, and these changes are interpreted to reflect variations in *GDS/A* ratio. FW, footwall; HW, hanging wall.

and 14C). Other examples are terminal tips of faults A, B, A′ and Z1 (Figs. 5, 9 and 11).

7.5.4. Faults with no expression at free surface (type IV tip)

Fault D represents an example of a buried fault that is not associated with growth strata (Fig. 7A). Platform-derived fills and early diagenetic fabrics within palaeocaverns developed along this fault provide evidence for its Capitanian age (Fig. 7A and C). It is therefore, interpreted to represent a syndepositional fault with a type IV upper termination (Fig. 14D). Fault Z2 represents another example of a fault tipping blindly within strata whose depositional topography has not been affected by contemporaneous faulting at depth. It is therefore also considered to have a type IV tip (Figs. 11, 12C and D).

7.6. GDS/A ratio and fault-tip morphology

Relationships between the upper fault tips and growth strata described in the above examples are essentially static. The structural styles of the faults have, however, evolved from one of the four types into another as the faults grew. These variations are thought to have occurred in response to temporal changes in the faults' *GDS/A* ratio. The four diagrams in Fig. 14 show how changes in *GDS/A* ratios are thought to have controlled structures associated with upper fault tips. Differential subsidence rates across faults breaching the depositional surface clearly must have exceeded the rates of contemporaneous platform aggradation. Type I fault terminations are therefore interpreted to have developed when *GDS/A* was greater than 1 (Fig. 14A). In the Capitan platform, such fault terminations only seem to have developed during sea-level lowstands, when limited deposition of terrestrial siliciclastics, or even non-deposition, took place on the subaerially exposed platform top. Type II fault terminations require a balance between *GDS* and *A*, and are therefore, interpreted to have occurred when *GDS/A* approximated 1 (Fig. 14B). Such fault terminations are considered to have developed during sea level highstands, when fault scarps on the flooded platform were readily covered by rapidly aggrading carbonate sediments. Burial of faults under growth monoclines, and ultimately under non-deformed strata, is thought to indicate a decrease in *GDS/A* ratio, either due to a decrease in fault-propagation rate, or increase in platform-aggradation rate, or both. Type III fault terminations are therefore interpreted to have developed when the *GDS/A* ratio was lower than 1 (Fig. 14C and D). Faults tipping out at depths too high to deform the contemporaneous free surface had *GDSS/A* ratio of 0.

7.7. Along-strike changes in fault-tip morphology

In addition to temporal changes, structures associated with upper fault tips also tend to vary laterally. This lateral heterogeneity is due mainly to the fact that faults in sedimentary rocks tend to have elliptical shapes, and therefore tip out at different depths along strike (e.g. Rippon, 1985; Barnett et al., 1987; Walsh and Watterson, 1988; Cowie and Scholz, 1992a,b; Cladouhos and Marett, 1996; Watterson et al., 1996). As a result, each section through a fault represents a unique structure, and has to be assessed individually. For example, the coupled exposures of fault/fracture zones E and A′ show distinctly different structures across North Slaughter Canyon (Figs. 8 and 9). Figs. 6 and 10 illustrate how structures associated with upper terminations of faults A, E and A′ are thought to have varied along strike at different stages of the fault development.

Structures of syndepositional faults and fractures in the Capitan platform as described in this paper may appear to be complex. However, Fig. 15 shows that faults and fractures can be easily characterised using structures associated with their upper terminations. Elsewhere, syndepositional faults and fractures can be described in terms of one of the four principal types of their upper tips defined in Fig. 14.

8. Discussion

8.1. Fault-tip structure: comparison with other studies

Various structural–stratigraphic studies observed an apparent relationship between relative rates of syntectonic deposition, and the depth and morphology of upper terminations of syndepositional faults (e.g. see examples and discussion in Bosence et al., 1998). Burchette (1988) and Cross et al. (1998) presented evidence that strata in the Miocene Gebel Abu Shaar syn-rift carbonate platform, Gulf of Suez, were at times disrupted by a major block-bounding extensional fault, while at other times the carbonate platform margin overgrew and sealed the fault (Bosence et al., 1998). Thus, the fault expressed itself as a scarp at the free surface, or was buried within the platform, in response to temporal variations in the growth-differential-subsidence/platform-aggradation ratio. Doglioni et al. (1998) stated that if sedimentation rate greatly exceeds differential subsidence rate, then faults only modify the geometry of syntectonic strata but do not affect their facies. Chronis et al. (1991) studied faults developed within the Quaternary fill of the Gulf of Patras, Greece. They observed faults growing at depth, with no facies change within contemporaneous strata deposited across them, and others that reached the free surface and were associated with facies change of the syntectonic strata. Similarly, Kkjennerud et al. (2001) studied Quaternary syndepositional faults in the Rukwa Rift, Tanzania, and identified faults tipping out at depth with no expression on the free surface, faults overlain by growth folds, faults associated with wedges of growth strata and reaching to free surface without any apparent expression on it, and faults with small scarps at free surface. Kkjennerud et al. (2001) linked the differing fault-tip morphologies to variations between the displacement rates and the contemporaneous depositional rates within the rift-formed Rukwa Lake. The upper-tip morphology of these faults, and of those discussed above, could be classified and interpreted according to terminology and response to *GDS/A* variations proposed in Fig. 14.

8.2. Quantitative data: comparison with other studies

Displacement and dimensions (e.g. length and width) represent the key static quantitative characteristics of faults (Walsh and Watterson, 1988). Displacement rate and instantaneous slip are, in turn, used to quantify fault growth in a dynamic sense. Two pieces of information are necessary to establish displacement rate: displacement and time over which a fault was active. Growth strata associated with syndepositional faults provide a measure that can be used to calculate the duration of fault activity. To date, most studies involving quantification of fault-displacement rates focused on large-scale tectonic faults related to crustal extension, such as those in the East African Rift System (Kkjennerud et al., 2001), east Mediterranean (Chronis et al., 1991; Roberts et al., 1993) and the Basin and Range Province of south-western USA (Machette et al., 1991). Displacement rates reported in these studies vary between 0.5 and 5 m/ka. Instantaneous slip is best observed at currently active faults that break the free surface. Instantaneous-slip throws of as much as 5 m at the free surface have been reported in literature (Machette et al., 1991; Leeder, 1995).

In this study, a different methodology has been chosen to quantify fault movement relative to deposition, whereby growth differential subsidence has been related to the thickness of contemporaneous growth strata accumulated within the more rapidly subsiding hanging walls of faults. This methodology is independent of estimation of rates of synkinematic deposition, which have been subject to debate (Borer and Harris, 1989, 1991, 1995; Ye and Kerans, 1996; Osleger, 1998; Tinker, 1998; Hunt et al., 2002) and represent an everlasting source of uncertainty. An earlier study by Hunt et al. (2002), however, calculated displacement rates of faults A–E on the eastern side of North Slaughter Canyon, using conservative estimates of 400 ka of the duration of the 4th-order sea-level cycles (Borer and Harris, 1991, 1995). Average displacement rate of 0.021 m/ka has been established for these faults, and are by 1–2 orders of magnitude lower than those reported for large extensional faults referred to above. An alternative choice of a shorter duration of the 4th-order sea-level cycles of 250 ka (Osleger, 1998) would resume in a proportionally higher fault-displacement rate of 0.034 m/ka. These would still be 1–2 orders of magnitude lower than displacement rates measured on the larger tectonic faults (refs. above). These quantifications might lead one to speculate that tectonic faulting driven by crustal extension occurs at a greater pace than shallow faulting driven by compaction. It may be that the different driving forces of faults developed within extensional settings and those studied here may be the reason for the different fault-displacement rates.

The present study established that differential subsidence across faults breaking free surface was, at all times, lower than platform aggradation rates during highstands of relative sea level (0.053–0.336 m/ka; Hunt et al., 2002). Bosence et al. (1998) argued that differential subsidence at free surface across tectonic faults (up to 5 m/ka) is lower than rise in sea level due to glacioeustasy (up to 14 m/ka). This relationship seems to be consistent with patterns of differential subsidence at free surface of syndepositional faults observed in the Capitan platform. Faults are found to have only able to form fault scarps during lowstands of sea

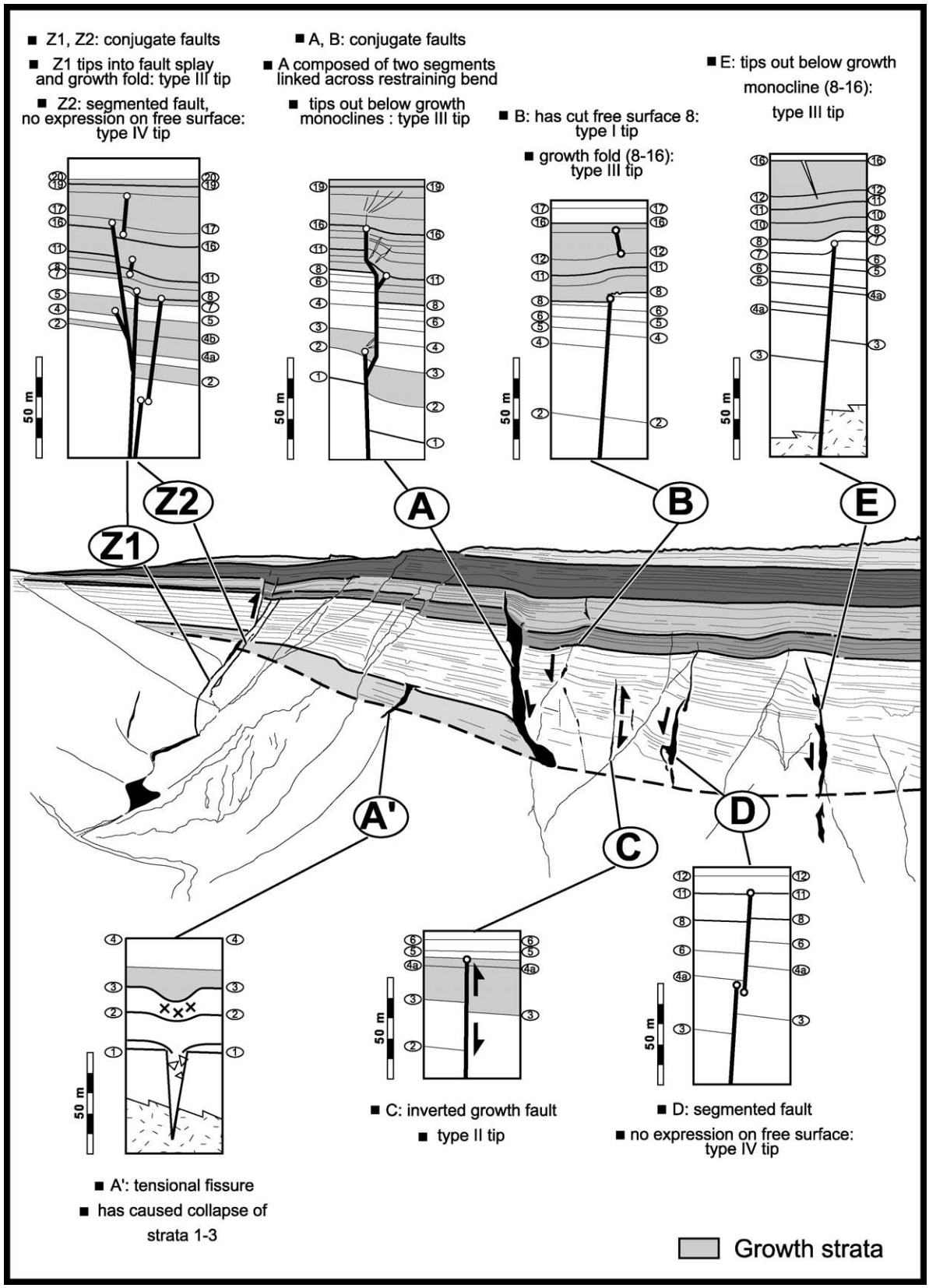

Fig. 15. Summary of structural characteristics of syndepositional faults and fractures on the east side of North Slaughter Canyon. Note that although structures associated with the upper fault tips are spatially and temporally variable, they can be elsewhere described in terms of the four structural types (I–IV) defined in Fig. 14.

level, and these were levelled and buried under younger strata with the onset of the rise of sea level associated with high-productivity carbonate deposition.

8.3. Implications for platform stratigraphy

The origin of the geometry of the outer part of the Capitan platform, whereby back-reef strata thicken and steepen toward the basin (Fig. 3), has been subject to long-standing debate. Specifically, the discussion revolves around a *primary/depositional* versus *secondary/compaction-related* origin of the platform geometry. To date, most studies have considered the basinward-thickening and dipping strata to have preserved the primary platform bathymetry that flattened through time and was solely controlled by depositional processes and sea-level changes (Dunham, 1972; Pray and Esteban, 1977; Yurewicz, 1977; Hurley, 1989; Kerans and Harris, 1993; Rankey and Lehrmann, 1996; Osleger, 1998; Tinker, 1998; Osleger and Tinker, 1999; Kerans and Tinker, 1999). Fewer studies have suggested a secondary, compaction-related origin of the strata geometry (Saller, 1996; Hunt and Fitchen, 1999; Longley, 1999; Hunt et al., 2002) showed that geopetals dip at up to 14° in the Seven Rivers strata, and flatten upwards, in common with bedding. This pattern is taken to prove the origin of the basinward steepening and thickening of the platform strata through syndepositional down-to-basin tilting. Differential compaction of underlying basinal deposits is inferred to have driven the tilting.

Two new lines of evidence arose from this study to indicate that the 'fall-in' geometry is a product of syndepositional tilting rather than being depositional in origin. Firstly, syndepositional faults and fractures are systematically developed where back-reef strata steepen and thicken abruptly basinward (Fig. 3). This observation, and the common strike of syndepositional faults and fractures with that of bedding, geopetals and platform margin (Figs. 1C and 2), are taken to indicate that the abrupt changes in dip of the strata are a result of deformation rather than deposition. Secondly, basinward-throwing faults are consistently steeper compared to shelfward-throwing faults, and locally show reverse orientation (e.g. A, C, A′, Z1; Figs. 5C, 7B, 9 and 11C). Some of the faults also show evidence for structural inversion as they developed (e.g. C, A′, Z1; Figs. 7A and 9A). The steeper dips, reverse sense of displacement, and local structural inversion of the originally basinward-throwing faults are consistent with basinward rotation of these faults in course of basinward tilting of the platform.

9. Conclusions

In Slaughter Canyon, Guadalupe Mountains, New Mexico, the Upper Permian Capitan platform is cut by syndepositional faults and fractures. The platform has a 'fall-in' geometry whereby strata thicken and steepen basinward. Faults are dip-slip, have displacements of up to 24 m, dip shelf- and basinward at angles higher than 75°, and are consistently parallel to depositional strike. Faults and fractures are systematically developed where steepening and thickening of strata is most pronounced. Shelfward-throwing faults are invariably normal, and dip at angles shallower than basinward-throwing faults. Basinward-throwing faults are mostly reverse, and some have changed their sense of displacement as they developed. These patterns indicate basinward rotation of these faults as they grew. The preferential development of faults and fractures within strata that steepen and thicken abruptly basinward, and the evidence for fault rotation, are considered to represent new evidence for the origin of the basinward-steepening geometry of the Capitan platform through syndepositional down-to-basin tilting.

Fault initiation and development was strongly influenced by two types of extensional fractures. First, faults appear to have been preferentially established along pre-existing fissures in the reef and back-reef strata. Second, fractures within fault-related growth monoclines appear to have directed propagation of faults through the platform strata. Some growth folds are interpreted to have developed over stable, or non-propagating, fault tips. Linkage of previously unconnected fault segments at depth is considered to have caused differential subsidence across faults, which induced growth folding without vertical propagation of the locked upper fault tips. Soft siliciclastics overlying the upper fault tips may have contributed to the preferred downward-pointed propagation and linkage of fault segments by absorbing some of the stress and acting as mechanostratigraphic barriers to upward fault growth.

Four types of faults are distinguished on the basis of structure of their upper termination: (I) faults that broke the free surface, (II) faults tipping out within non-folded growth strata, (III) shallowly buried faults tipping out below growth monoclines, and (IV) buried faults with no expression on the free surface. Faults changed temporarily from one type into another, depending on contemporaneous variations in the *GP/A* ratio. Fault-tip structures are also observed to have varied laterally, and these variations are explained to have reflected the distance from the fault centre.

Acknowledgements

This paper is based on part of E. Koša's PhD thesis accepted by the University of Manchester in 2003. The PhD was sponsored by Total and Norsk Hydro, and this support is gratefully acknowledged. Marie-Odile Bockel-Rebelle, Gerald Roberts and Enzo Insalaco helped to develop ideas presented in this paper through inspiring discussions in the field. Reviews and comments by Jaume Vergés, Joao Hippertt and an anonymous reviewer helped to improve the manuscript. In New Mexico and Texas we are thankful for invaluable support from Fred Armstrong and Gorden Bell of

the Guadalupe Mountains National Park, and Renee West and Paul Burger of the Carlsbad Caverns National Park. E. Koša is indebted to the Dionýz Štúr Geological Institute of Slovakia for financial support during his studies in Manchester.

References

Anders, M.H., Schlische, R.W., 1994. Overlapping faults, intrabasin highs, and the growth of normal faults. Journal of Geology 102, 165–180.

Barnett, J.A.M., Mortimer, J., Rippon, J.H., Walsh, J.J., Watterson, J., 1987. Displacement geometry in the volume containing a single normal fault. American Association of Petroleum Geologists Bulletin 71, 925–937.

Bertram, G.T., Milton, N.J., 1989. Reconstructing basin evolution from sedimentary thicknesses: the importance of palaeobathymetric control, with reference to the North Sea. Basin Research 1, 247–257.

Borer, J.M., Harris, P.M., 1989. Depositional facies and cycles in Yates Formation outcrops, Guadalupe Mountains, New Mexico. In: Harris, P.M., Grover, G.A. (Eds.), Subsurface and Outcrop Examination of the Capitan Shelf Margin, Northern Delaware Basin Society of Economic Paleontologists and Mineralogists, Core Workshop, vol. 13, pp. 305–317.

Borer, J.M., Harris, P.M., 1991. Lithofacies and cyclicity of the Yates Formation, Permian Basin: implications for reservoir heterogeneity. American Association of Petroleum Geologists Bulletin 75, 726–779.

Borer, J.M., Harris, P.M., 1995. Computer simulation of the Yates Formation (Permian, Delaware Basin)—sequence stratigraphy and shelf-to-basin correlation implications. In: Martin, R.L. (Ed.), In search of new Permian oil and gas fields: using today's technologies and tomorrow's ideas for exploration, development and 3D seismic in a mature basin West Texas Geological Society, Publication, vol. 95–98, pp. 111–132.

Bosence, D.W.J., Cross, N., Hardy, S., 1998. Architecture and depositional sequences of Tertiary fault-block carbonate platforms; an analysis from an outcrop (Miocene Gulf of Suez) and computer modelling. Marine and Petroleum Geology 15, 203–221.

Burchette, T.P., 1988. Tectonic control on carbonate platform facies distribution and sequence development: Miocene, Gulf of Suez. Sedimentary Geology 59, 179–204.

Childs, C., Nicol, A., Walsh, J.J., Watterson, J., 1996. Growth of vertically segmented normal faults. Journal of Structural Geology 18, 1389–1397.

Chronis, G., Piper, D.J.W., Anagnostou, C., 1991. Late Quarternary evolution of the Gulf of Patras, Grece: tectonism, deltaic sedimentation and sea-level change. Marine Geology 97, 191–209.

Cladouhos, T.T., Marett, R., 1996. Are fault growth and linkage models consistent with power-law distributions of fault lengths? Journal of Structural Geology 18, 281–293.

Cowie, P.A., Scholz, C.H., 1992a. Displacement–length scaling relationship for faults: data synthesis and discussion. Journal of Structural Geology 14, 1149–1156.

Cowie, P.A., Scholz, C.H., 1992b. Physical explanation for the displacement–length relationship of faults using a post-yield fracture mechanics model. Journal of Structural Geology 14, 1133–1148.

Cross, N.E., Purser, B.H., Bosence, D.W.J., 1998. The tectono-sedimentary evolution of a rift margin fault-block carbonate platform: Abu Shaar, Gulf of Suez, Egypt. In: Purser, B.H., Bosence, D.W.J. (Eds.), Sedimentation and tectonics of rift basins: Red Sea–Gulf of Aden. Chapman and Hall, London, pp. 271–295.

Doglioni, C., D'Agostino, N., Mariotti, G., 1998. Normal faulting versus regional subsidence and sedimentation rate. Marine and Petroleum Geology 15, 737–750.

Dunham, R.J., 1972. Capitan Reef, New Mexico and Texas: Facts and Questions to aid Interpretation and Group Discussion. Society of Economic Paleontologists and Mineralogists, Publication 72–14, 297pp.

Erdlac Jr., R.J., 1993. Small-scale structures in the Guadalupe Mountains region; implication for Laramide stress trends in the Permian basin. In: Love, D.W., Hawley, J.W., Kues, B.S., Adams, J.W., Austin, G.S., Barker, J.M. (Eds.), Carlsbad Region, New Mexico and West Texas New Mexico Geological Society, 44th Annual Field Conference, pp. 167–174.

Ferrill, D.A., Stamatakos, J.A., Sims, D., 1999. Normal fault corrugations: implications for growth and seismicity of active normal faults. Journal of Structural Geology 21, 1027–1038.

Fischer, A.G., Sarnthein, M., 1988. Airborne silts and dune-derived sands from the Permian of the Delaware basin. Journal of Sedimentary Petrology 58, 637–643.

Garber, R.A., Grover, G.A., Harris, P.M., 1989. Geology of the Capitan shelf margin-subsurface data from the northern Delaware Basin. In: Harris, P.M., Grover, G.A. (Eds.), Subsurface and Outcrop Examination of the Capitan Shelf Margin, Northern Delaware Basin Society of Economic Paleontologists and Mineralogists, Core Workshop, vol. 13, pp. 3–271.

Gawthorpe, R.L., Leeder, M.R., 2000. Tectono-sedimentary evolution of active extensional basins. Basin Research 12, 195–218.

Gawthorpe, R.L., Fraser, A.J., Collier, R.E.L., 1994. Sequence stratigraphy in extensional basins: implications for the interpretation of ancient basin-fills. Marine and Petroleum Geology 11, 642–658.

Gawthorpe, R.L., Sharp, I., Underhill, J.R., Gupta, S., 1997. Linked sequence stratigraphic and structural evolution of propagating normal faults. Geology 25, 795–798.

Graziano, R., 2000. The Aptian–Albian of the Apulia Carbonate Platform (Gargano Promontory, southern Italy): evidence of palaeoceanographic and tectonic controls on the stratigraphic architecture of the platform margin. Cretaceous Research 21, 107–126.

Hardy, S., McClay, K., 1999. Kinematic modelling of extensional fault-propagation folding. Journal of Structural Geology 21, 695–702.

Harwood, G.M., Kendall, A., 1999. Reef nargin collapse, gully formation and filling within the Permian Capitan Reef: Carlsbad Caverns, New Mexico, USA. Sedimentology 46, 443–441.

Hayes, P.T., 1964. Geology of the Guadalupe Mountains, New Mexico, United States Geological Survey, Professional Paper, 446 1964, p. 69.

Hill, C.A., 1996. The Geology of the Delaware Basin, Guadalupe, Apache and Glass Mountains New Mexico and west Texas, Society of Economic Paleontologists and Mineralogists, Permian Basin Section, Special Publication, vol. 96–39 1996, p. 480.

Hill, C.A., 2000. Overview of the Geologic history of cave development in the Guadalupe Mountains, New Mexico. Journal of Cave and Karst Studies 62, 60–71.

Horsfield, W.T., 1977. An experimental approach to basement-controlled faulting. Geologie en Mijnbouw 56, 363–370.

Hunt, D.W., Fitchen, W.M., 1999. Compaction and the dynamics of carbonate platform development: insights from the Permian Delaware and Midland basins, southeast New Mexico and west Texas, USA. In: Harris, P.M., Saller, A.H., Simo, J.A. (Eds.), Advances in Carbonate Sequence Stratigraphy: Application to Reservoirs, Outcrops and Models Society of Economic Paleontologists and Mineralogists, Special Publication, vol. 63, pp. 75–106.

Hunt, D.W., Fitchen, W.M., Koša, E., 2002. Syndepositional deformation of the Permian Capitan Reef carbonate platform, Guadalupe Mountains, New Mexico, USA. Sedimentary Geology 154, 89–126.

Hurley, N.F., 1989. Facies mosaic of the lower Seven Rivers Formation, McKittrick Canyon, New Mexico. In: Harris, P.M., Grover, G.A. (Eds.), Subsurface and Outcrop Examination of the Capitan Shelf Margin, Northern Delaware Basin Society of Economic Paleontologists and Mineralogists Core Workshop, vol. 13, pp. 325–346.

Jackson, J., McKenzie, D., 1983. The geometrical evolution of normal fault systems. Journal of Structural Geology 5, 471–482.

Jagnow, D.H., Jagnow, R.R., 1992. Stories from rocks; the geology of the Guadalupe Mountains, Carlsbad, Carlsbad Caverns–Guadalupe Mountains Association 1992. 40pp.

Kerans, C., Harris, P.M., 1993. Outer shelf and shelf crest. In: Bebout, D.G., Kerans, C. (Eds.), Guide to Permian Reef Geology Trail, McKittrick Canyon, Guadalupe Mountains National Park, West Texas Guidebook, vol. 26. Bureau of Economic Geology, University of Texas, Austin, pp. 32–43.

Kerans, C., Tinker, S.W., 1999. Extrinsic stratigraphic controls on development of the Capitan Reef complex. In: Saller, A.H., Harris, P.M., Kirkland, B.L., Mazzullo, S.J. (Eds.), Geological Framework of the Capitan Reef Society of Economic Paleontologists and Mineralogists, Special Publication, vol. 65, pp. 15–36.

Kerans, C.K., Fitchen, W.M., Gardner, M.H., Sonnenfeld, M.D., Tinker, S.W., Wardlaw, B.R., 1992. Styles of sequence development within uppermost Leonardian through Guadalupian strata of the Guadalupe Mountains, Texas and New Mexico. In: Murk, D.H., Curan, B.C. (Eds.), Permian Basin Exploration and Production Strategies: Applications and Sequence Stratigraphic and Reservoir Characterization Concepts West Texas Geological Society, Symposium 92–91, pp. 1–7.

Kkjennerud, T., Lippard, S.J., Vanhauwaert, P., 2001. Short term development of intracontinental rifts, with reference to the late Quarternary of the Rukwa Rift (East African Rift System). Marine and Petroleum Geology 18, 307–317.

Koša, E., Hunt, D.W., Fitchen, W.M., Bockel-Rebelle, M.-O., Roberts, G., 2003. The heterogeneity of Paleocavern systems developed along Syndepositional Faults; Upper Permian Capitan platform, New Mexico, USA. In: Ahr, W.M., Harris, P.M., Morgan, W.A., Somerville, I.D. (Eds.), Permo-Carboniferous Carbonate Platforms and Reefs Society of Economic Paleontologists and Mineralogists, Special Publication 78 and American Association of Petroleum Geologists, Memoir, vol. 83, pp. 291–322.

Leeder, M.R., 1995. Continental rifts and proto-oceanic troughs. In: Busby, C.J., Ingersoll, R.V. (Eds.), Tectonics of sedimentary basins. Blackwell Science, pp. 119–148.

Leeder, M.R., Gawthorpe, R.L., 1987. Sedimentary models for extensional tilt-block/half-graben basins. In: Coward, M.P., Dewey, J.F., Hancock, P.L. (Eds.), Continental extensional tectonics Geological Society, London, Special Publication, vol. 28, pp. 139–152.

Longley, A.J., 1999. Differential compaction and its effects on the outer shelf of the Permian Capitan Reef Complex, Guadalupe Mountains, New Mexico. In: Saller, A.H., Harris, P.M., Kirkland, B.L., Mazzullo, S.J. (Eds.), Geological framework of the Capitan Reef Society of Economic Paleontologists and Mineralogists, Special Publication, vol. 65, pp. 85–106.

Machette, M.N., Persounis, S.F., Nelson, A.R., 1991. The Wasatch fault zone-Utah-segmentation and history of Holocene earthquakes. Journal of Structural Geology 13, 137–149.

Mazzullo, S.J., Mazzullo, J., Harris, P.M., 1985. Eolian origin of quartzose sand sheets in Permian shelf facies, Guadalupe Mountains. In: Cunninghamm, B.K., Hedrick, C.L. (Eds.), Permian carbonate/clastic sedimentology, Guadalupe Mountains—analogs for shelf and basin reservoirs Society for Sedimentary Geology, Permian Basin Section, Special Publication Core Workshop, vol. 85–24, p. 71.

Meissner, F.F., 1972. Cyclic sedimentation of middle Permian strata of the Permian Basin. In: Elam, J.G., Chuber, J. (Eds.), Cyclic sedimentation in the Permian Basin, 2nd ed. West Texas Geological Society, Midland, pp. 203–232 (publication 72–60).

Melim, L.A., Scholle, P.A., 2002. Dlomitization of the Capitan formation forereef facies (Permian, west Texas and New Mexico): seepage reflux revisited. Sedimentology 49, 1207–1227.

Muraoka, H., Kamata, H., 1983. Displacement distribution along minor fault traces. Journal of Structural Geology 5, 483–495.

Osleger, D.A., 1998. Sequence architecture and sea-level dynamics of Upper Permian shelfal facies, Guadalupe Mountains, southern New Mexico. Journal of Sedimentary Research 68, 327–346.

Osleger, D.A., Tinker, S.W., 1999. Three-dimensional architecture of upper Permian high-frequency sequences, Yates-Capitan shelf margin, Permian Basin, USA. In: Harris, P.M., Saller, A.H., Simo, J.A. (Eds.), Advances in carbonate Sequence Stratigraphy: Application to Reservoirs, Outcrops and Models Society of Economic Paleontologists and Mineralogists, Special Publication, vol. 63, pp. 169–185.

Peacock, D.C.P., Sanderson, D.J., 1991. Displacement, segment linkage and relay ramps in normal fault zones. Journal of Sedimentary Geology 15, 721–733.

Peacock, D.C.P., Sanderson, D.J., 1996. Effects of propagation rate on displacement variations along faults. Journal of Structural Geology 18, 311–320.

Pray, L.C., Esteban, M., 1977. Upper Guadalupian facies, Permian reef complex, Guadalupe Mountains, New Mexico and west Texas. In: Hileman, M.E., Mazzullo, S.J. (Eds.), Upper Guadalupian facies, Permian Reef Complex, Guadalupe Mountains, New Mexico and West Texas Society of Economic Paleontologists and Mineralogists, Permian Basin Section, Publication, vol. 77–16. 194pp.

Rankey, E.C., Lehrmann, D.J., 1996. Anatomy and origin of toplap in a mixed carbonate-clastic system, Seven Rivers Formation (Permian, Guadalupian), Guadalupe Mountains, New Mexico, USA. Sedimentology 43, 807–826.

Rippon, J.H., 1985. Contoured patterns of the throw and hade of normal faults in the Coal Measures (Westphalian) of northwest Derbyshire. Proceedings of the Yorkshire Geological Society 45, 147–161.

Roberts, G.P., Gawthorpe, R.L., Stewart, I., 1993. Surface faulting in active normal fault zones: examples from the Gulf of Corinth fault system. Zeitschrift für Geomorphologie, N.F. Supplement 94, 303–328.

Rosales, I., 1999. Controls on carbonate platform evolution on active fault blocks: the Lower Cretaceous Castro Urdiales platform (Aptian, Albian, Northern Spain). Journal of Sedimentary Research, Section B: Stratigraphy and Global Studies 69, 447–465.

Rosales, I., Fernandez, M.P.A., Garcia, M.J., 1994. Carbonate depositional sequence development on active fault blocks: the Albian in the Castro Urdiales area, northern Spain. Sedimentology 41, 861–882.

Saller, A.H., 1996. Differential compaction and basinward tilting of the prograding Capitan reef complex, Permian, west Texas and southeast New Mexico, USA. Sedimentary Geology 101, 21–30.

Saller, A.H., Harris, P.M., Kirkland, B.L., Mazzullo, S.J. (Eds.), 1999. Geological Framework of the Capitan Reef Society of Economic Paleontologists and Mineralogists, Special Publication, vol. 65, p. 224.

Sarg, J.F., 1988. Carbonate sequence stratigraphy. In: Wilgus, C.K., Hastings, B.S., Kendall, C.G.St.C., Posamentier, H.W., Ross, C.A., Van Wagoner, J.V. (Eds.), Sea-Level Changes: An Integrated Approach Society of Economic Paleontologists and Mineralogists, Special Publication, vol. 42, pp. 155–181.

Schlische, R.W., Anders, M.H., 1996. Stratigraphic effects and tectonic implications of the growth of normal faults and extensional basins. In: Berata, K. (Ed.), Reconstructing the History of the Basin and Range Extension using Sedimentology and Stratigraphy Geological Society of America, Special Paper, vol. 303, pp. 183–203.

Tinker, S.W., 1998. Shelf-to-basin facies distributions and sequence stratigraphy of a steep-rimmed carbonate margin: Capitan depositional system, McKittrick Canyon, New Mexico and Texas. Journal of Sedimentary Research 68, 1146–1174.

Vergés, J., Marzo, M., Muñoz, J.A., 2002. Growth strata in foreland settings. Sedimentary Geology 146, 1–9.

Walsh, J.J., Watterson, J., 1988. Analysis of the relationship between displacements and dimensions of faults. Journal of Structural Geology 10, 239–247.

Walsh, J.J., Watterson, J., 1992. Populations of faults and fault displacements and their effects on estimates of fault-related regional extension. Journal of Structural Geology 14, 701–712.

Walsh, J.J., Watterson, J., Bailey, W.R., Childs, C., 1999. Fault relays, bends and branch-lines. Journal of Structural Geology 21, 1019–1026.

Watterson, J., Walsh, J.J., Gillespie, P.A., Easton, S., 1996. Scaling systematics of fault sizes on a large-scale range fault map. Journal of Structural Geology 18, 199–214.

Wibberley, C.A.J., Petit, J.P., Rives, T., 1999. Mechanics of high displacement gradient faulting prior to lithification. Journal of Structural Geology 21, 251–257.

Wilson, M.E.J., 1999. Prerift and synrift sedimentation during early fault segmentation of a Tertiary carbonate platform, Indonesia. Marine and Petroleum Geology 16, 825–848.

Withjack, M.O., Olson, J., Peterson, E., 1990. Experimental models of extensional forced folds. American Association of Petroleum Geologists Bulletin 74, 1038–1054.

Ye, Q., Kerans, C., 1996. Reconstructing Permian eustasy from 2-D backstripping and its use in forward models. In: DeMis, W.D., Cole, A.G. (Eds.), The Brushy Canyon Play in Outcrop and Subsurface: Concepts and Examples Society of Economic Paleontologists and Mineralogists, Permian Basin Section, Publication, vol. 96–38, pp. 69–74.

Yurewicz, D.A., 1977. The origin of the massive facies of the lower and upper Capitan Limestone (Permian), Guadalupe Mountains, New Mexico and west Texas. In: Hileman, M.E., Mazzullo, S.J. (Eds.), Upper Guadalupian facies, Permian Reef Complex, Guadalupe Mountains, New Mexico and West Texas Society of Economic Paleontologists and Mineralogists, Permian Basin Section, Publication, vol. 77–16, pp. 45–92.